Chapter 5

The Morphology of Stoichiometric Ceria Crystallites

5.1 Introduction

Surfaces play a crucial role in many of the chemical and physical processes that involve the reaction of inorganic oxides and their environment, such as catalysis and crystallisation. Indeed, it is clear that even the shape or morphology of a crystallite is controlled by the surface properties. Despite this, the number of experimental studies concerning the atomic structure of insulating surfaces has been limited, while those that have been carried out have concentrated primarily on the low index faces [115, 116]. Nevertheless, new developments such as atomic force microscopy and improvements in existing techniques are set to change the present situation [117]. The computer simulation of surfaces is also proving to be a very useful technique in furthering our understanding of processes occurring at the atomistic level. In combination with experimental techniques, such simulations can provide details of

the crystal morphology, energetics, surface structure, surface composition, and the effect of adsorbents on the surface.

Previous surface simulations of CeO_2 have primarily concentrated on the low index faces [27, 28]; in the present chapter we explicitly model a far greater range of unique faces. The surfaces we choose to examine are the unique (hkl) indices where $h^2+k^2+l^2 < 20$. In addition, we provide some evidence that by considering this extensive range of surfaces we may be in a position to extrapolate to other high index faces. Given the number of low coordinate edge and corner like surface sites on such high index faces, they are likely candidates to explain the catalytic behaviour of ceria, and will certainly be present in the polycrystalline material used commercially. This can be seen from Figure 5.1, a HREM image of commercial grade CeO_2, which shows evidence of a variety of grains and crystallites, some of which are facetted.

We note that similar studies have been carried out on NiO by Yan *et al.* [118]. In that work, the series of planes from (100) to (110), the (1a0) series, were studied and the smooth change in surface energy as a function of "a" noted. However, the surfaces in the NiO study were non-dipolar, that is none of these surfaces had a dipole moment in the z-direction [119]. Conversely, in the present study, a number of dipolar surfaces have been studied. The significance of this difference is discussed in section 5.4.

In addition to studying a variety of faces, this work compares the dependence of the results on the choice of interatomic potential. Each set of potentials is based on a fully ionic description of the lattice. However, the three potentials differ in their ability to reproduce various physical properties of the bulk lattice. Given this, the present chapter considers the enduring problem of the applicability and transferability,

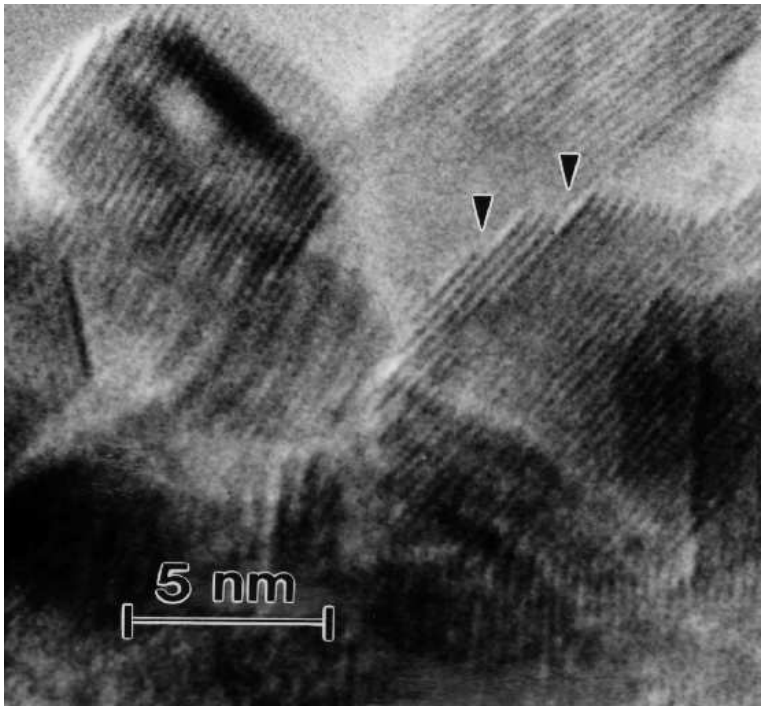

Figure 5.1: HREM image of commercial CeO_2, the arrows show the presence of surface facets. The material was supplied by Johnson-Matthey plc, the micrograph was taken by Dr. M. A. McCoy, Dept. of Materials, Imperial College.

to surface studies, of pair potentials derived from bulk properties.

5.2 Methodology

5.2.1 Simulation Techniques

The atomistic surface simulation techniques described previously are used throughout the present chapter. The surfaces were generated from a CeO_2 lattice that had previously been minimised in the bulk lattice program GULP. The surface code MARVIN was then used to 'cleave' the lattice at the prescribed point and to relax the newly formed surface. The region I size was set to approximately 25Å and the region II size

set to 35Å.

In Chapter Two we discussed the use of the shell model to account for the polarisability of the lattice. In certain situations such as surfaces, additions can be made to the model to stabilise the structure. These higher order terms can be understood by considering the restoring force on the spring;

$$F = k_1 \delta r + \frac{1}{6} k_2 \delta r^3 + ... \tag{5.1}$$

where k_1 refers to the harmonic constant (stiffness) and k_2 the fourth order anharmonic contribution of the spring (these are fourth order terms in the Taylor expansion of the energy of displacement). Usually, only the k_1 term is used; however, in certain cases a k_2 term must be used to prevent unphysical polarisations of the shell. Such situations generally occur in systems with large electric fields and where the ion species are very polarisable. Fourth order terms have been used in the present work for some of the surfaces. The technique entails using the smallest value possible for the k_2 term that prevents the shells from becoming displaced by more than a given amount (0.7Å in the present study). Clearly, the need for an anharmonic term implies some inadequacy in the modelling of polarisability.

5.2.2 Potential Parameters

It was found that the potential parameters for ceria used in the previous chapter and in other studies [27, 28, 11] could not model the more complex high index faces such as the (322), (311), and (331). In particular, these potentials permitted unphysically large relaxations of the surface resulting in the separation of the oxygen shells from their cores. This being the case, two new Ce^{4+} - O^{2-} potentials were derived by

empirical fitting. They were based on an oxygen - oxygen potential which has been shown previously to be particularly robust for surface studies [59], and for simulations of complex defect structures in bulk materials [72]. In addition to deriving new potentials, the original Butler potentials were used with a k_2 term on the oxygen shell for the more complex surfaces. It was shown, by empirical means, that the a k_2 value of 5000eVÅ^{-4} was sufficient to prevent the shell displacement becoming excessive. For potentials 1 and 2 on several of the high index faces, the initial part of the minimisation was carried with an anharmonic term. The k_2 term was then removed and relaxation continued. Such a technique permits the system to effectively be 'guided' along the potential energy hyper-surface and prevents it following unphysical paths.

The potential parameters are listed in Table 5.1; in Table 5.2 we compare, with experiment, the bulk properties derived using these potentials. All three sets of potentials give good results for the crystal structure of ceria. However potential 1 gives a very low theoretical value for the oxygen ion migration energy (via a vacancy migration mechanism). Conversely, both the Butler potential and potential 2 yield migration energies in good agreement with the experimentally well defined value of 0.7eV$\pm$ 0.1eV [6, 120]. Unfortunately, potential 2 was unable to reproduce the static dielectric constant to a good degree of accuracy.

In Table 5.3 we compare the energies for various intrinsic disorder reactions in CeO_2. The relative order of the energies calculated by all three potentials is the same, i.e. the choice of potential has very little effect upon the overall outcome, but it does play a role in the absolute energies of reaction. Potential 2 gives the highest values for the reaction energies, while the Butler potential the lowest. The effect of

Interaction	A (eV)	ρ (Å^{-1})	C (eVÅ^6)	Shell Parameters			
					k (eVÅ^{-2})	Y (e)	
$O^{2-} - O^{2-}$	9547.92	0.2192	32.00	O^{2-}	9.3	-2.04	Potential 1
$Ce^{4+} - O^{2-}$	1809.68	0.3547	20.40	Ce^{4+}	177.84	-0.20	
$O^{2-} - O^{2-}$	9547.92	0.2192	32.00	O^{2-}	10.3	-2.04	Potential 2
$Ce^{4+} - O^{2-}$	2531.5	0.335	20.40	Ce^{4+}	177.84	-0.20	
$O^{2-} - O^{2-}$	22764.3	0.149	43.83	O^{2-}	419.9	-6.10	Butler
$Ce^{4+} - O^{2-}$	1986.8	0.3511	20.40	Ce^{4+}	291.8	7.7	

Table 5.1: Potential Parameters

the potential choice on the surface energy is discussed in Section 5.6.

5.3 Calculating crystal morphologies

The shape of a crystal can be determined by two methods; resulting in the equilibrium and growth morphologies respectively. The former morphology is that which reduces the total surface energy of the crystal to a minimum for a given volume [122]. Therefore, the morphological importance of a face is inversely related to the surface energy. The growth morphology is based on measurement of the energies associated with the deposition of molecules/unit cells upon all of the competing surfaces; growth morphologies will be dominated by the surface with the least negative attachment energy [123] as the faster growing faces (i.e. those with the most negative attachment energies) effectively grow themselves out of existence [124].

Surface Energy The surface energy is defined as the energy required per unit area to create a surface by cleaving the bulk crystal (see Figure 5.2) and displacing the

Property	Potential 1	Potential 2	Butler	Experiment
Lattice Energy (eV)	-105.65	-106.70	-105.65	Unknown
Lattice Constant ($\AA$)	5.411	5.411	5.411	5.411
Static Dielectric (ϵ_0)	18.60	12.71	19.53	18.6 - 20.0
High Frequency Dielectric (ϵ_∞)	4.54	3.98	4.00	4.0
Elastic Constants (C_{11}, x10^{11}Dynes cm^{-2})	55.42	57.30	50.44	40.3[105]
Elastic Constants (C_{12}, x10^{11}Dynes cm^{-2})	12.46	14.77	14.31	10.5
Elastic Constants (C_{44}, x10^{11}Dynes cm^{-2})	12.36	14.68	1.61	6.0
Bulk Modulus (x10^{11}Dynes cm^{-2})	26.79	28.94	26.36	23.6[121]
Shear Modulus (x10^{11}Dynes cm^{-2})	21.50	21.26	18.07	14.9
Oxygen Migration Energy (eV)	0.30	0.59	0.74	0.7$\pm$0.1

Table 5.2: Comparison of the calculated and experimental lattice properties for the three potentials

	Potential 1	**Potential 2**	**Butler**
$V_O^{\bullet\bullet}$	15.40	16.54	16.06
$V_{Ce}^{\prime\prime\prime\prime}$	85.44	87.74	83.52
$O_i^{\prime\prime}$	-8.99	-9.23	-10.43
$Ce_i^{\bullet\bullet\bullet\bullet}$	-63.18	-62.11	-65.80
Schottky Energy per defect	3.54	4.71	3.33
Anion Frenkel Energy per defect	3.21	3.66	2.81
Cation Frenkel Energy per defect	11.13	12.82	8.86

Table 5.3: Comparisons of energies (in eV) for disorder reactions for the three potential sets

two surfaces to an infinite distance apart. Formally, the definition is

$$\gamma(hkl) = \frac{E_{Total}(hkl) - E_{Boundary}(hkl) - nE_{Crystal}}{A} \tag{5.2}$$

where n is the number of unit cells in region I and A is the surface area of the simulation cell. $E_{Crystal}$ is the lattice energy, E_{Total} the total energy of region I, and $E_{Boundary}$ is the interaction energy of the region I/region II boundary.

Attachment Energy The attachment energy is the energy released per molecule, when a growth slice of thickness d_{hkl} is attached to an existing crystal surface, (*hkl*), (Figure 5.3). Mathematically it can be expressed as,

$$E_{Attach}(hkl) = E_{Crystal} - E_{Sl}(hkl) \tag{5.3}$$

where E_{Sl} is the energy of all the ions within the slice (*hkl*). This quantity is one measure of the rate of growth on that face. As such, the attachment energy concerns the kinetic evolution of surfaces; hence a prediction of the growth morphology can be derived from this quantity. Such crystals are dominated by the slowest growing faces, i.e. those planes whose attachment energies are closest to zero.

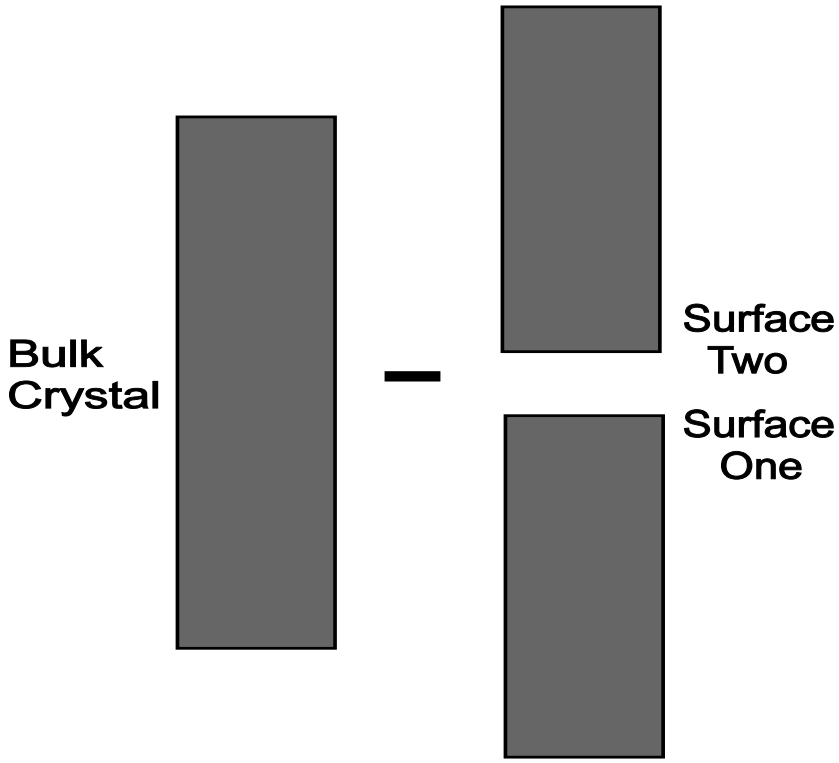

Figure 5.2: Surface Energy

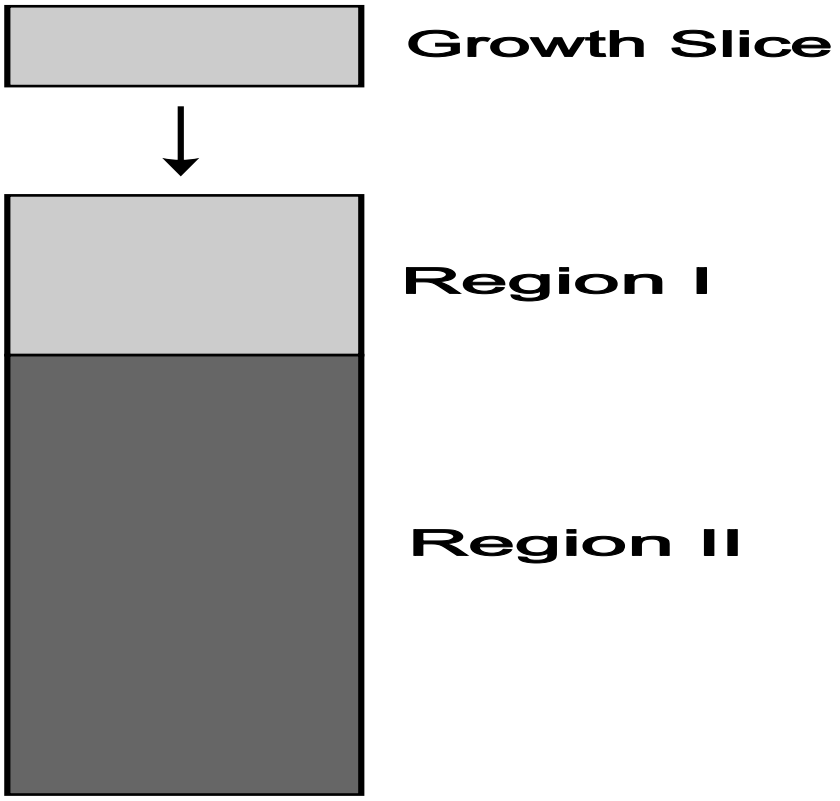

Figure 5.3: Attachment Energy

5.4 Surface Types

The presence of a particular surface in a morphology and the proportion of the total surface area it occupies is dependent on the absolute stability of the respective surface.

A stable surface will form only if the Madelung sums can converge as a function of increasing crystal thickness. One practical limitation this imposes is that a surface is required to be electrically neutral and not possess a dipole moment perpendicular to the surface [55]. It has been shown [119] that when such a dipole exists the surface is unstable and will have an energy which increases dramatically with crystal thickness.

The physical basis for this is that when such a dipole is created, two effective charges reside on the two opposing surfaces. Thus as the width of the slab increases so does the dipole energy which prevents the surface from growing.

This has led to the classification of inorganic surfaces into three types, according to their atomic arrangements (Figure 5.4) [55].

Type I faces are surfaces whose cations and anions are in the same plane and hence can be terminated at any plane in the unit cell.

Type II surfaces consist of charged ion planes which are arranged symmetrically. Consequently the surface can only be terminated at specific points along the unit cell otherwise a significant dipole perpendicular to the surface results. In CeO_2 the type II surfaces consist of a neutral three plane repeat unit.

Type III surfaces consist of alternating layers of cations and anions. Consequently, irrespective of where along the unit cell the surface is terminated, there is a dipole in the z-direction. Such faces can only form if defects are created on the surface.

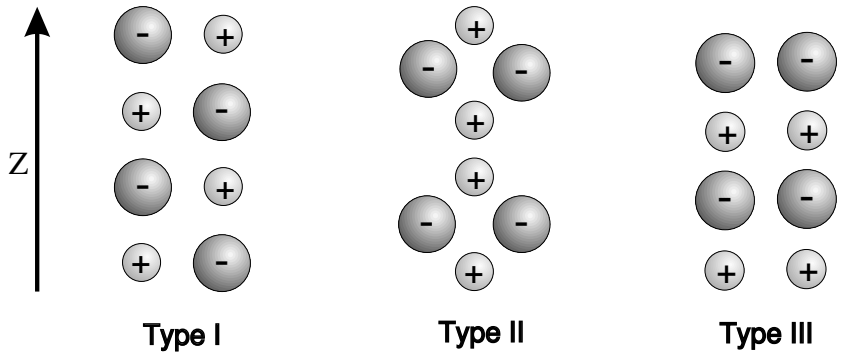

Figure 5.4: Classification of surfaces

5.5 Stabilisation of dipolar surfaces

Dipolar surfaces cannot be simulated unless the dipole is removed from the surface, either through the movement of ions or the creation of electronic defects. Thus the dipole is neutralised by the creation of a second dipole, which is in an equal and opposite direction to the first; the resulting net dipole is therefore zero. In the present study such dipoles are created by the movement of ions. This is achieved by either moving half the ions from the top of region I to the bottom of region II (vacancy stabilisation) or the converse, where half the ions from the bottom of region II are moved to the top of region I (interstitial stabilisation) (Figure 5.5). This process effectively turns the type III surface into a type II surface.

Once the dipole has been removed it is imperative to ensure the same number of ions are present in region I. Hence, adjustments must be made to the region I/region II interface and the relevant number of ions added or subtracted from region I.

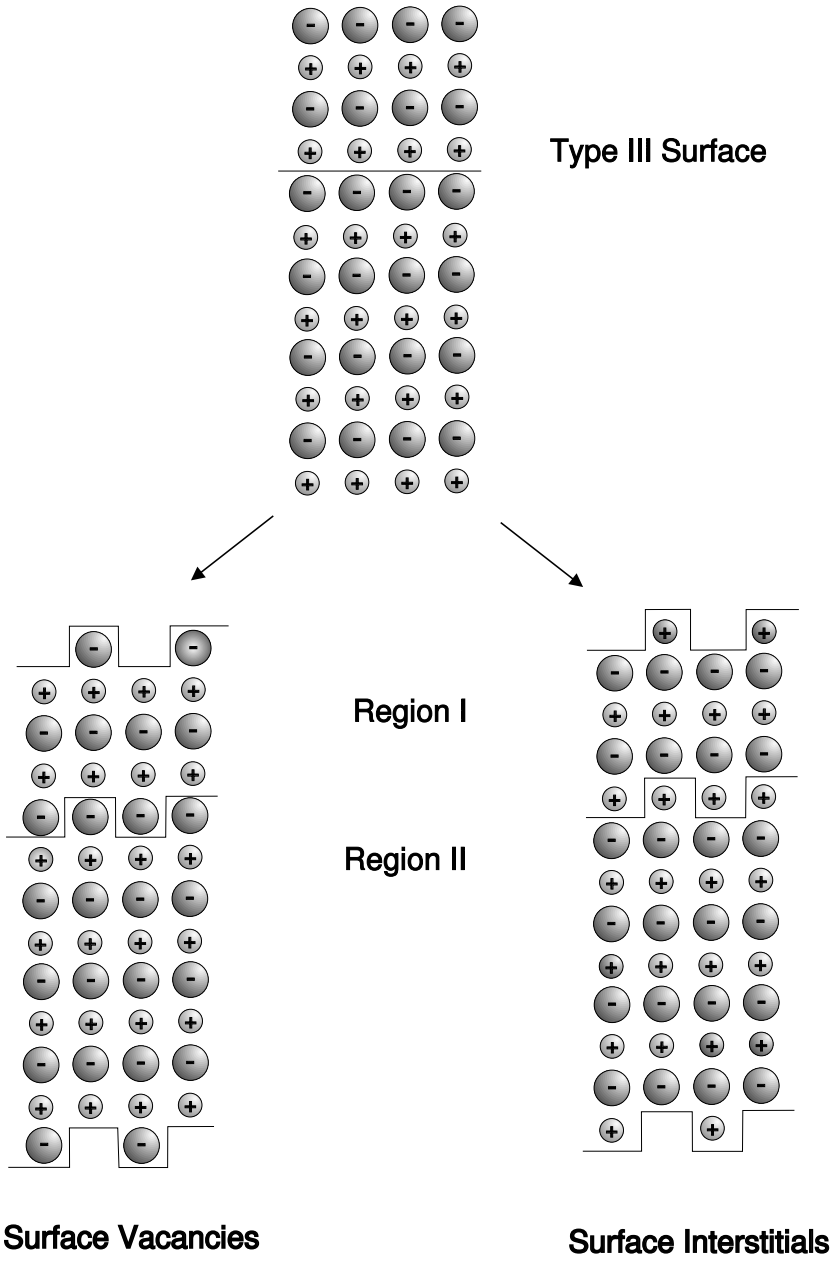

Figure 5.5: Neutralisation of a dipole on a Type III surface

5.6 Surface Energies

The criteria for choosing the faces to study was that the Miller planes satisfied the expression $h^2 + k^2 + l^2 < 20$. Table 5.4 lists the surface energies for these planes, and for the three sets of potentials; before and after relaxation. The cut is defined as where along the unit cell the surface is terminated. In the case of a type III surface this can be either on a cation plane or an anion plane.

The most stable face at equilibrium is the (111) surface, irrespective of the potential, both before and after relaxation. The greatest relaxations are seen for type III faces, which tend to undergo significant rearrangements as they contain defects on the surface which stabilise them. It is important to note that for any given surface, all three potential models yield unrelaxed surface energies that are practically identical (Table 5.4). The same is true for the attachment energies (Table 5.5). This would be expected given that all three potentials are fitted to the same lattice properties and, in particular, give very similar results for the perfect lattice energies.

Figures 5.8 and 5.9 show the surface energies for the (11a) and the (01a) family of planes. They are plotted as a function of the misorientation angle, which in the case of the (11a) family is the angle the respective surface plane makes with the (110) plane. Figure 5.6 shows the change in the angle as one goes from a (11 $\frac{1}{2}$) plane (the (221) plane) to a (111) plane. Figure 5.7 defines the misorientation angle for the (01a) family of planes.

The (11a) family The curves of the three potentials all show a distinct minimum at 45° which corresponds to the (111) plane. The energy difference between potential 1 and potential 2 is smallest at 45°. The increase in this difference as one moves

		Potential 1		**Potential 2**		**Butler Potential**	
Surface	Cut	Unrelaxed	Relaxed	Unrelaxed	Relaxed	Unrelaxed	Relaxed
(111)	0.50	1.63	1.35	1.82	1.55	1.72	1.21
(200)	0.125 (A)	9.04	3.01	9.35	3.92	9.11	2.18
	0.125(B)	6.31	2.90	6.62	3.54	6.45	2.01
	0.375(C)	11.73	4.03	12.04	4.74	11.71	2.25
(210)	0.125 (A)	5.70	2.45	5.97	2.94	$5.75^{\dagger}$	1.56
	0.125 (B)	5.68	2.41	5.95	2.93	$5.74^{\dagger}$	1.70
	0.375	10.54	3.25	10.80	2.97	$10.55^{\dagger}$	2.20
(211)	0.25	$6.81^{\dagger}$	2.37	7.05	2.97	$6.85^{\dagger}$	1.75
(220)	0.25	3.55	2.13	3.78	2.44	3.61	1.57
(221)	0.125	12.91^{*}	1.69	13.45^{*}	1.95	$12.84^{\dagger}$	1.31
	0.375	8.68^{*}	2.30	8.94^{*}	1.95	$8.73^{\dagger}$	1.73
(310)	0.25	11.59	3.52	11.87	4.30	$11.59^{\dagger}$	1.96
(311)	0.75	7.82	2.70	8.10	3.43	$7.85^{\dagger}$	2.02
(320)	0.125	11.53	2.31	15.33^{*}	4.09	$11.72^{\dagger}$	2.38
	0.375	5.04	2.31	5.29^{*}	2.74	$5.09^{\dagger}$	1.55
(321)	0.50	5.58	1.84	5.82	2.68	$5.62^{\dagger}$	1.42
(322)	0.125	11.58^{*}	1.93	11.84^{*}	2.38	$11.62^{\dagger}$	1.70
	0.375	$9.89^{\dagger}$	2.71	$10.14^{\dagger}$	3.35	$9.92^{\dagger}$	1.84
(331)	0.50	3.03	1.78	3.25	2.09	$3.10^{\dagger}$	1.27
(410)	0.125	13.62^{*}	2.68	13.90	3.47	$13.63^{\dagger}$	1.72
	0.375	$17.94^{\dagger}$	3.26	18.22	4.24	$17.93^{\dagger}$	2.17
(411)	0.50	12.31	2.96	12.57	3.67	$12.30^{\dagger}$	2.05

Table 5.4: Surface Energies (in Jm^{-2}) - * - Initially minimised using a k_2 term, which was later removed, † - Minimised using a k_2 term - see section 5.2 for more details

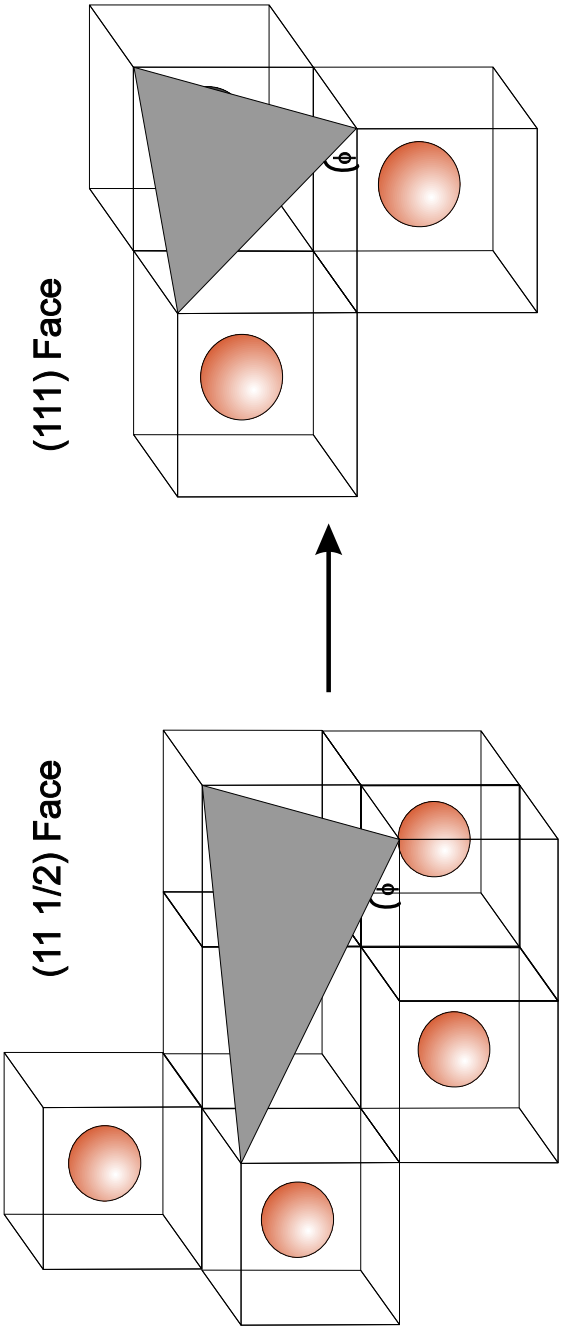

Figure 5.6: The misorientation angle for the (11a) planes

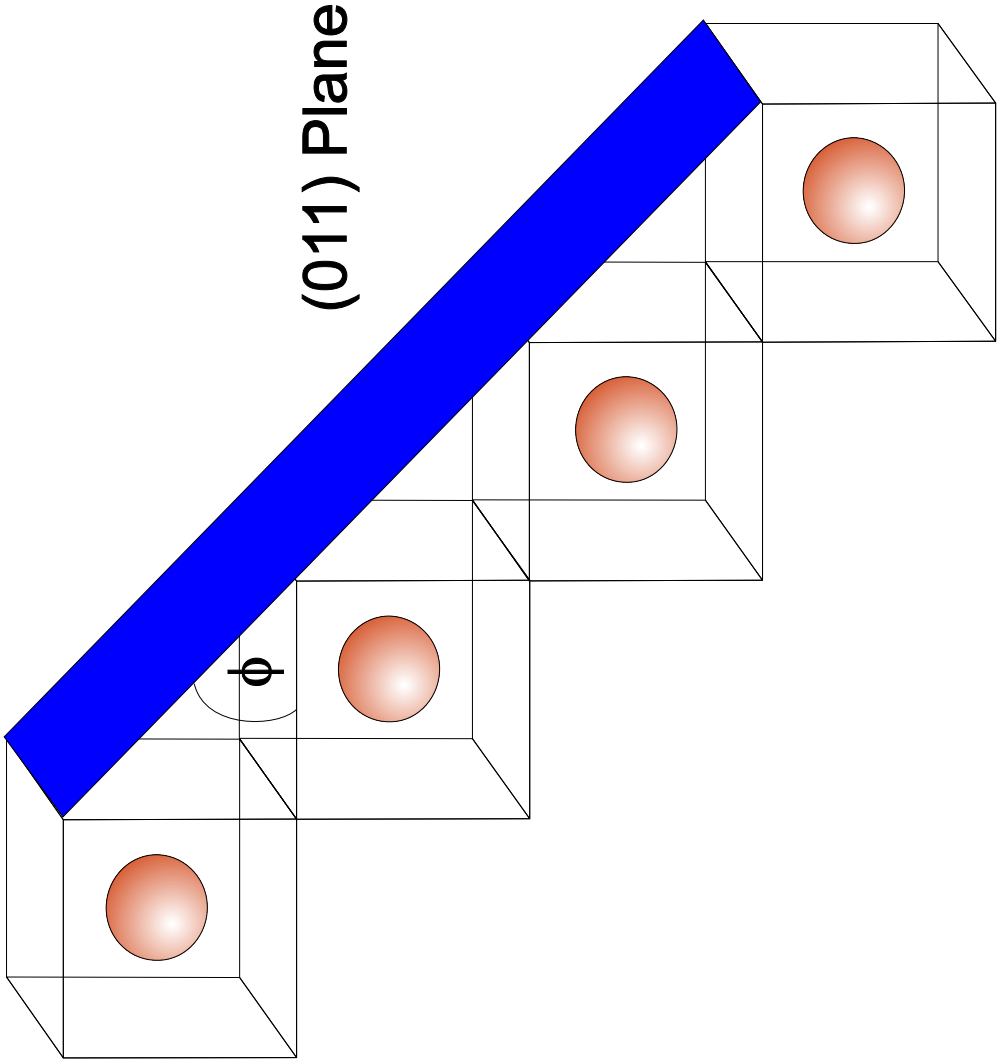

Figure 5.7: The misorientation angle for the (01a) planes

away from this angle is related to the effect the cerium-oxygen interaction has on the surface energy, since the Coulombic contribution and the oxygen-oxygen potential are the same for both sets. Although the Butler potential is based on a different oxygen - oxygen potential, it still shows a similar pattern. However, the gradients of the Butler curves are lower and hence the minimum is shallower. As with the Schottky and Frenkel disorder reactions the Butler model gives lower surface energies than the other two potentials.

The (01a) family This curve like the (11a) series shows a minimum at 45° irrespective of the potential used. However the (310) face is at a higher energy than either the (210) or (410) faces. The reason for this is related to the number of bonds broken to form the surface (see section 5.12). Similar treatments in NiO [56, 118] show a monotonic variation for the (01a) family of planes. However, these studies have only looked at type I surfaces. We on the other hand, have included all three surface types in our study, and yet we still see a well defined variation of energy with misorientation angle.

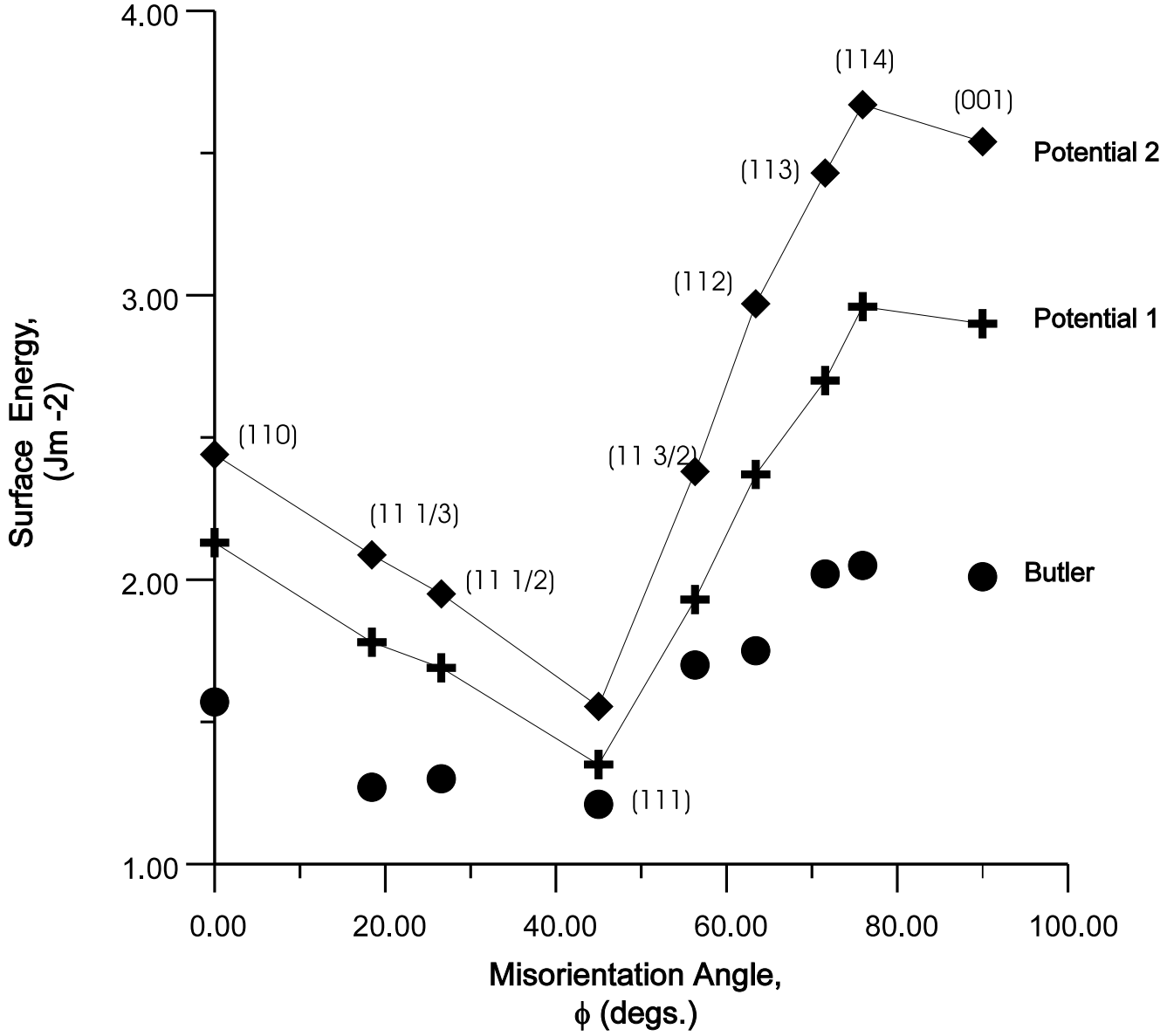

Figure 5.8: The surface energy as a function of ϕ for the (11a) direction

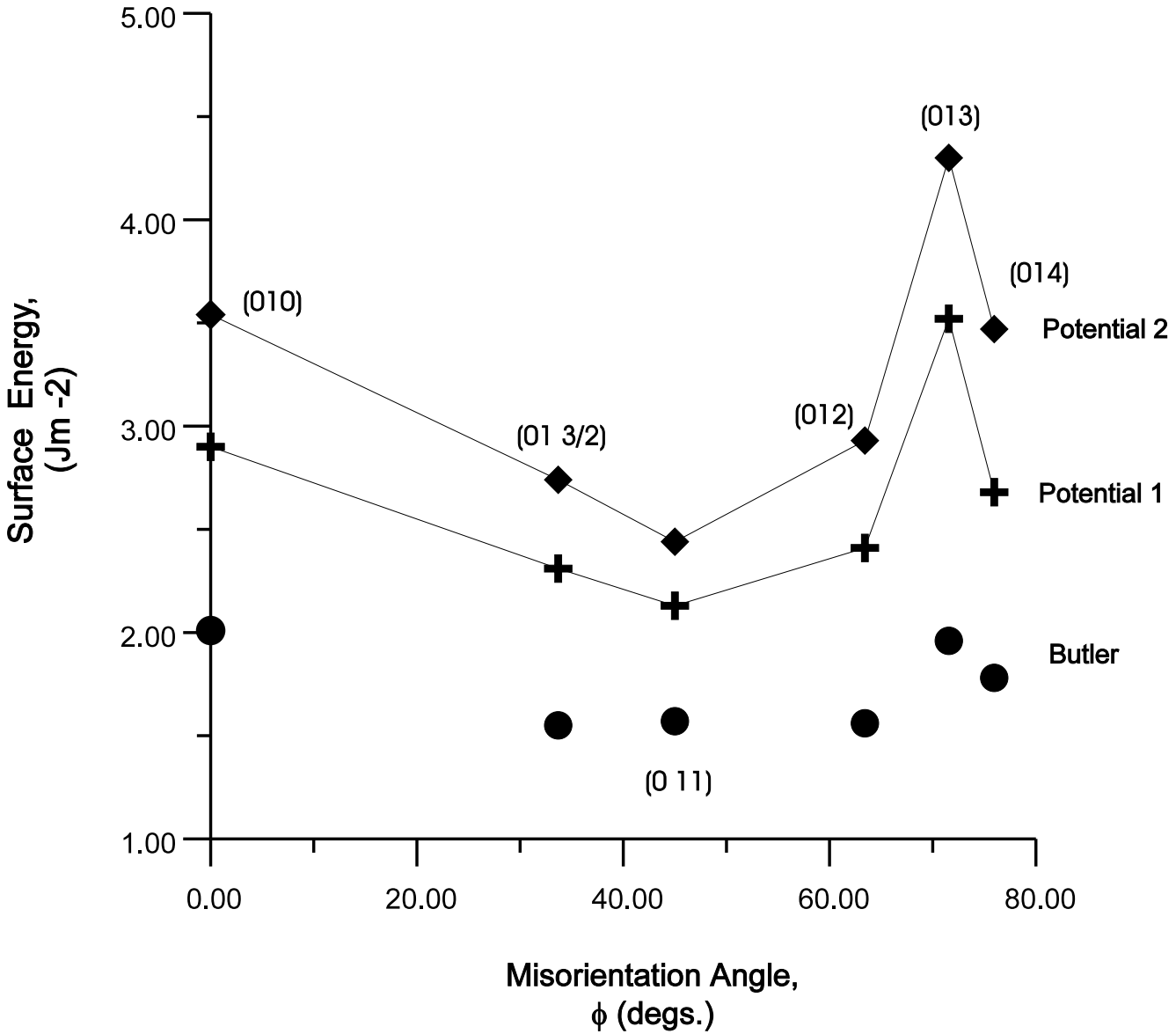

Figure 5.9: The surface energy as a function of ϕ for the (01a) direction

		Potential 1		**Potential 2**		**Butler**	
Surface	Cut	Unrelaxed	Relaxed	Unrelaxed	Relaxed	Unrelaxed	Relaxed
(111)	0.50	-2.58	-3.08	-2.87	-3.31	-2.71	-3.03
(200)	0.125 (A)	-14.72	-12.81	-15.27	-13.97	-14.83	-16.56
	0.125(B)	-16.65	-18.12	-17.13	-17.81	-16.65	-18.12
	0.375(C)	-20.84	-21.31	-21.39	-21.88	-20.79	-21.54
(210)	0.125 (A)	-12.58	-12.05	-13.12	-12.47	-12.67 †	-13.23
	0.125 (B)	-13.22	-13.25	-13.76	-13.47	-13.30†	-12.23
	0.375	-26.73	-33.43	-27.26	-40.13	-26.74†	-17.68
(211)	0.25	-19.01†	-25.07	-19.55	-25.46	-19.10†	-13.66
(220)	0.25	-43.85	-57.23	-23.03	-28.23	-22.13	-40.88
(221)	0.125	-30.47*	-7.38	-31.06*	-7.68	-30.80†	-27.41
	0.375	-31.97*	-35.60	-32.67*	-27.73	-31.53†	-48.91
(310)	0.25	-47.74	-46.34	-48.54	-47.14	-47.65†	-48.91
(311)	0.75	-33.20	-46.47	-34.00	-43.46	-33.18†	-34.45
(320)	0.125	-13.47	-21.63	-4.53*	-23.39	-13.81 †	-16.73
	0.375	-36.64	-42.21	-37.36*	-41.77	-36.67†	-44.60
(321)	0.50	-21.49	-37.88	-22.16	-28.47	-21.60†	-17.73
(322)	0.125	-47.74*	-23.50	-57.58*	-23.37	-56.96†	-64.00
	0.375	-27.22†	-28.99	-44.35†	-57.99	-43.74†	-59.24
(331)	0.50	-9.55	-14.32	-10.11	-13.98	-9.72†	-20.17
(410)	0.125	-75.04*	-36.23	-75.96	-59.63	-74.97†	-52.56
	0.375	-90.51†	-58.44	-91.43	-133.08	-102.22†	-130.29
(411)	0.50	-60.15	-74.81	-61.07	-75.30	-60.06†	-32.06

Table 5.5: Attachment Energies - (eV/mol.) * - Initially minimised using a k_2 term, which was later removed, † - Minimised using a k_2 term - see section 5.2 for more details

5.7 Attachment Energies

Table 5.5 shows the attachment energies for the three potentials. From the table it clear that the (111) surface, in addition to being the most thermodynamically stable, is also the slowest growing of the surfaces. This result, as with the surface energies, is independent of the potential used.

Figure 5.10 is a plot of these relaxed energies in the (11a) direction. In the case of the potentials 1 and 2, the attachment energy dependence on the misorientation

angle is similar to that seen for the surface energies. However, now of course, instead of a minimum energy at 45°, corresponding to the most favoured surface, we see a maximum value (i.e. that closest to zero) at 45°. Although the Butler potentials also gives rise to attachment energies with a maximum at 45°, the other attachment energies show no clear trend. This must be a consequence of relaxation effects, which are discussed in greater detail in section 5.11.

For the (01a) series, again we find the three potentials give similar attachment energies before relaxation (see Table 5.5). However, after relaxation, the energies do not reproduce the trends seen for the surface energies (Figure 5.11).

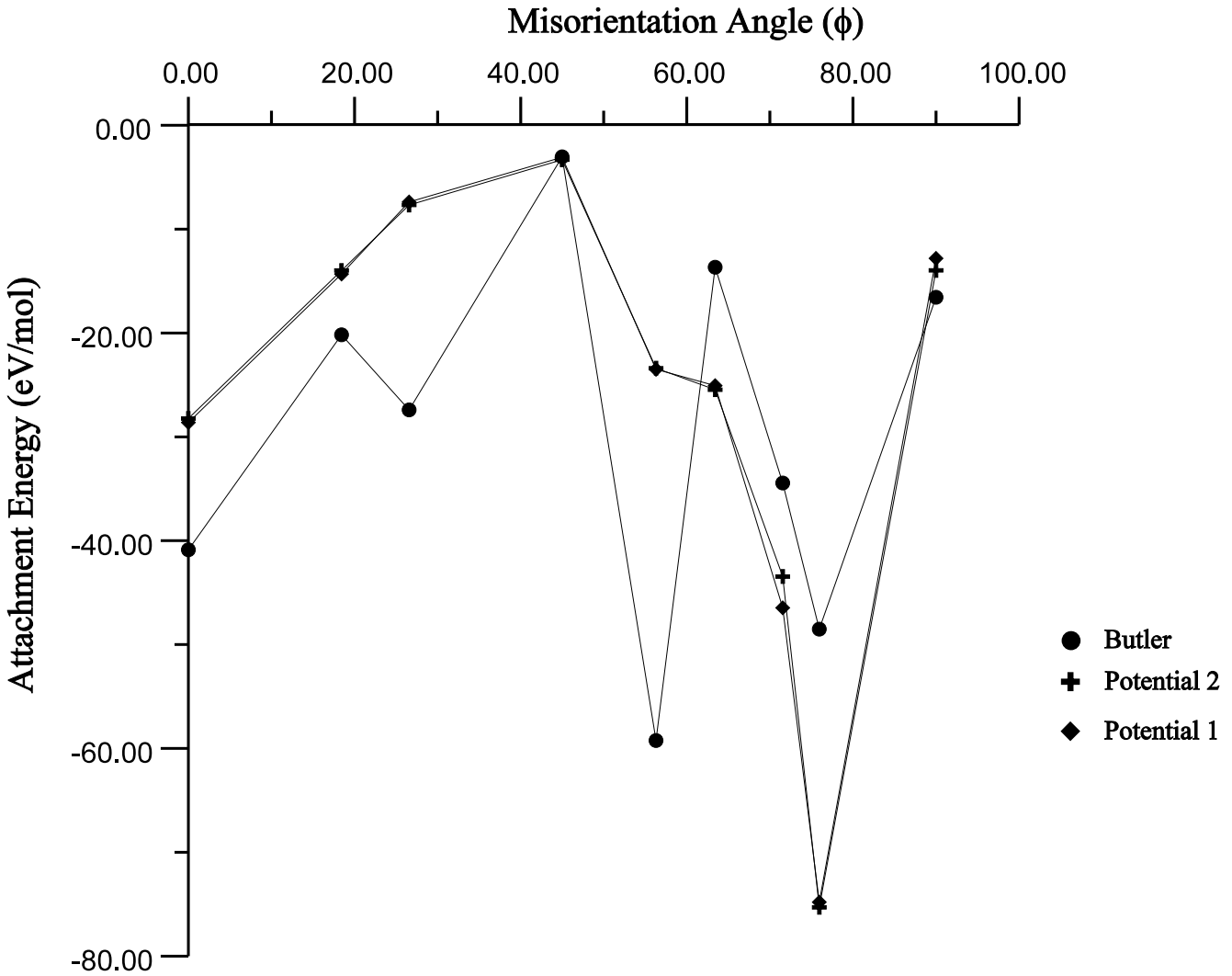

Figure 5.10: The relaxed attachment energy as a function of ϕ for the (11a)

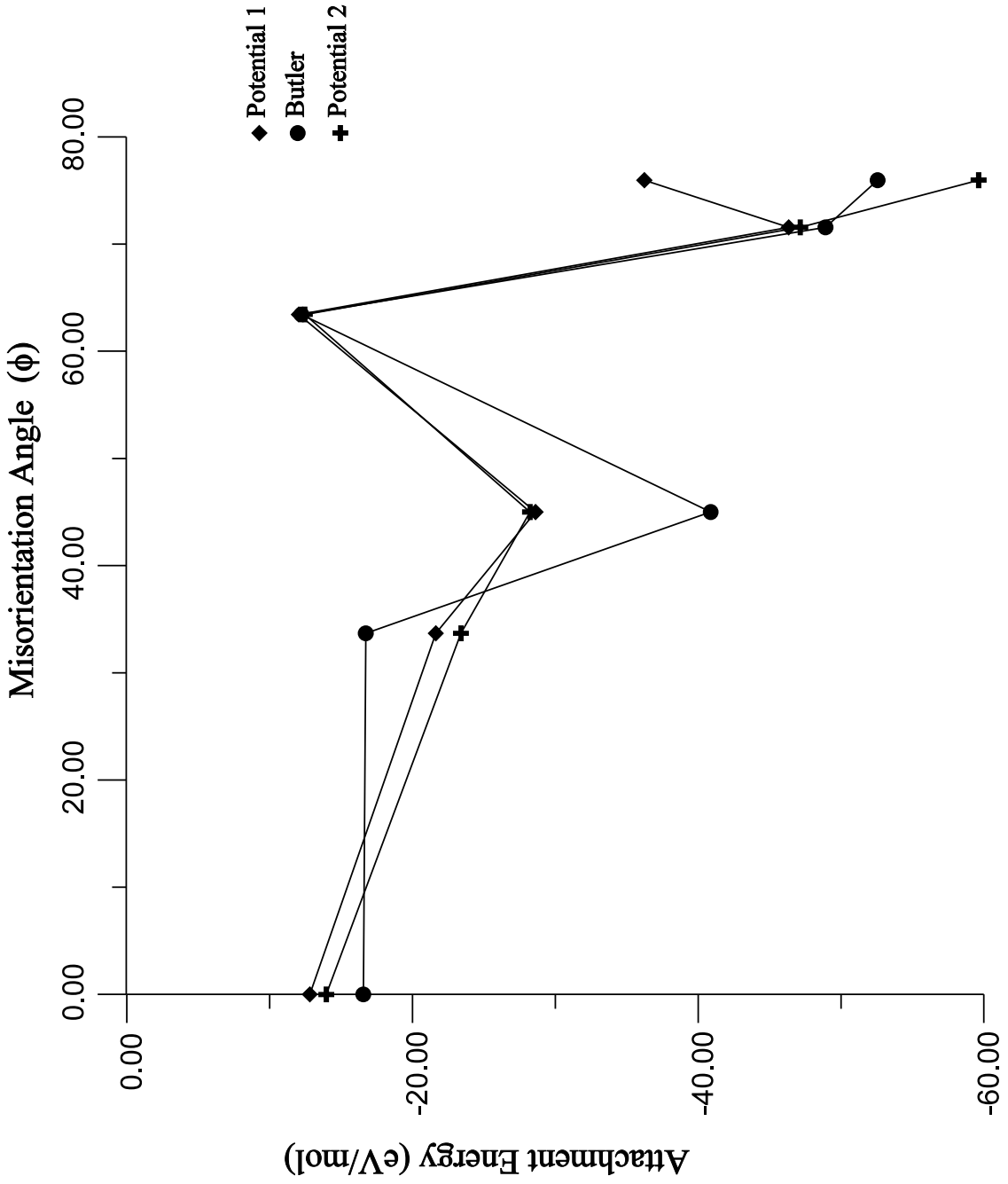

Figure 5.11: The relaxed attachment energy as a function of ϕ for the (01a)

5.8 Morphology

From our previous discussion of the surface and attachment energies in 5.6 and 5.7 respectively, it is possible to predict the growth and equilibrium morphologies of the crystals by using a Wulff treatment [**?**] (Figure 5.12).

Both potential 1 and potential 2 have growth and equilibrium morphologies entirely dominated by the (111) face. Conversely, the equilibrium morphology for the Butler potentials is different; as with the previous two equilibrium morphologies it has an overall octahedral shape. However, it also shows the presence of (331) and (210) facets. This difference in morphology can be attributed to the use of a k_2 term in the minimisation procedure. For a given potential model, such an anharmonic term will prevent a surface, which is inherently unstable, from unphysical core/shell displacements but still allow an excessively large polarisation energy. Such surfaces may therefore appear to be more significant in the morphology than is physically justifiable.

When single crystals of ceria are grown experimently the observed morphologies match our predicted morphologies [125]. If however, the crystals are grown substoichiometriclly their morphology is cubic [126]. This would be consistent with the non-stoichiometric growing conditions favouring the (200) surface which being a type III surface already accommodates a defect like structure.

5.9 Structure and Relaxation

Clearly it is important to consider not only the energetics of these surfaces but also their atomic structure. As a discussion of all the planes studied would be unfeasable

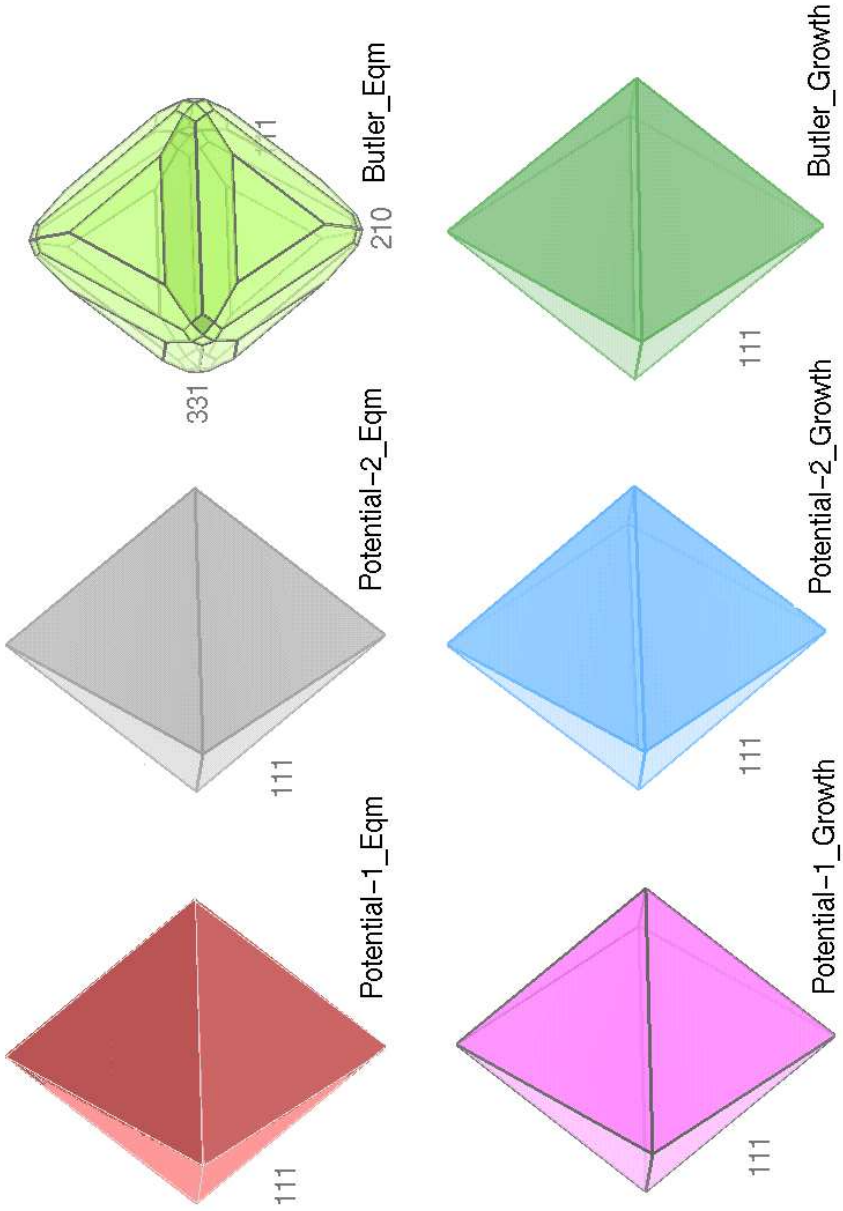

Figure 5.12: The crystal morphology of cerium oxide

we restrict our analysis to three important faces, the (111) and (200) faces which are seen experimentally, and the (331) face which is seen in the predicted Butler equilibrium morphology.

The (111) plane This is a type II surface and has four possible terminations within the unit cell of length, a; two are non-dipolar and equivalent, the other two are dipolar and also equivalent. The non-dipolar terminations are at the 0.5a and 0.75a positions along the unit cell. In fact, there is very little relaxation of this surface from the perfect cleaved geometry (see Figure 5.13) which is also evident from the remarkably small relaxation energy (about 0.3 Jm^{-2} for potential 1).

The two dipolar terminations of the (111) plane are the 0.125a and the 0.875a cuts. Their dipoles were neutralised by creating surface defects. However, despite eliminating the dipole the ion positions remained unstable with respect to convergence, indicating that the surface wishes to reconstruct. For reference, the unrelaxed surface energies of these terminations were 39.37Jm^{-2} and 34.69Jm^{-2} respectively, compared with 1.63Jm^{-2} for the non-dipolar cuts.

The (200) plane This is a type III surface and has two possible terminations; the 0.125a cut (a surface terminated by a cation plane) or the 0.375 cut (corresponding to termination by an anion plane). The 0.125 cut can be neutralised by either creating oxygen interstitial ions (identical to creating oxygen vacancies on the 0.375 cut) or by creating cerium vacancies on the surface (equivalent to cerium interstitials on the 0.375 cut). A third possibility is introduced since the oxygen interstitials on the surface can be configured in two ways, shown in Figure 5.14 (A and B).

In general, there is a significant movement and polarisation of ions on the surface

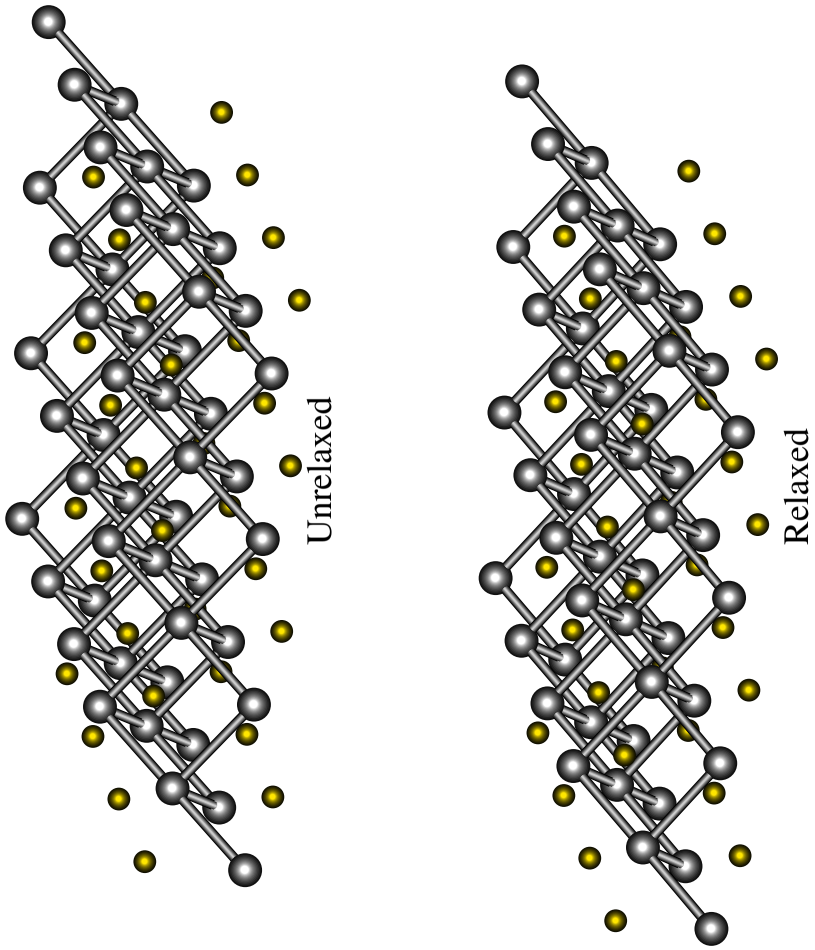

Figure 5.13: Surface structure of the (111) surface

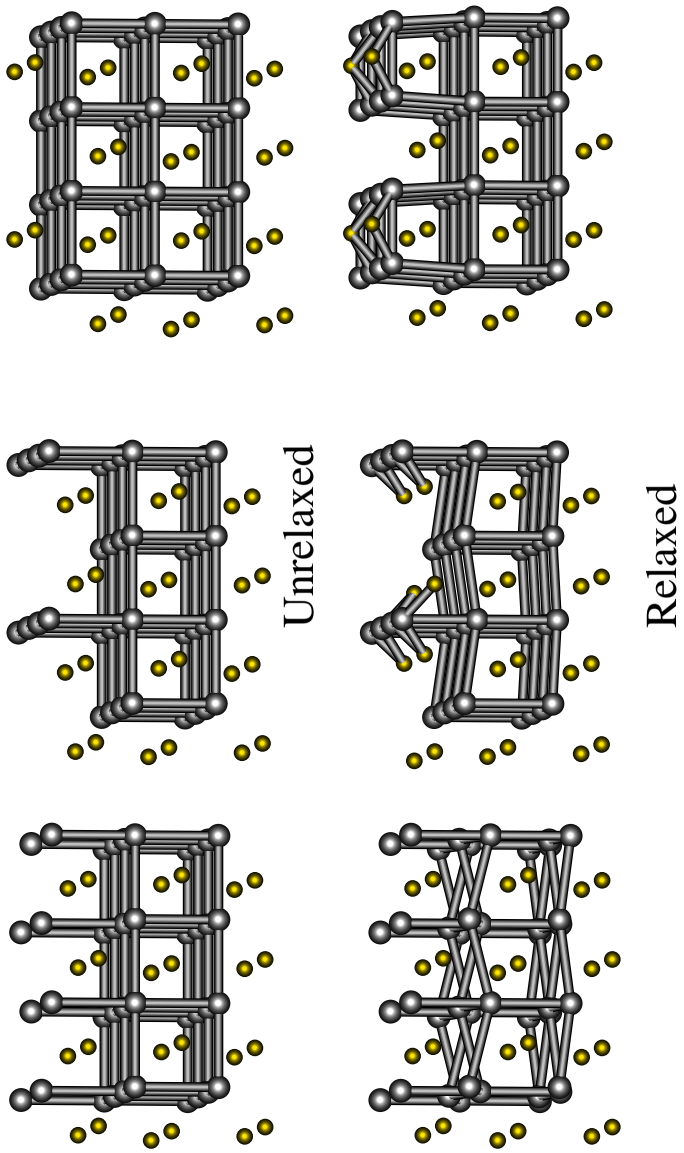

Figure 5.14: Surface structure of the (200) surface, and the method of neutralising the dipole

for both of the terminations. In all cases the uppermost layers move significantly downwards due to the Coulombic attraction of the oppositely charged ions in the plane below. The movement of the surface ions closer to the layer below also improves their coordination. This increasing of surface ion coordination has been seen in the simulation of other oxide surfaces such as MgO [127].

Configuration A (see Figure 5.14) has the lowest surface energy for the 200 plane; however, it does not have the lowest attachment energy. The smaller surface energy is due to the dipole neutralising oxygen interstitial ions being further apart, thus reducing the repulsion between the ions.

The relaxed surface structure of configuration A shows that the oxygen ions in the planes below the surface interstitial ions relax in an alternate upwards and downwards fashion; those directly below the interstitial ions relax downwards, with the extent of relaxation decreasing rapidly as a function of depth. On the other hand, those ions not below the interstitial relax upwards. The displacement upwards in the first layer is quite large (a change of 12.6% from the original position), in the subsequent layers the relaxation decreases very rapidly. The cerium ions exhibit negligible movement, with the exception of the surface layer which shows a uniform relaxation upwards of about 4%. Due to the symmetry of the surface there is no driving force for relaxation of the cerium ions in the xy plane.

Configuration B is the slowest growing surface configuration. The extent of the relaxation of the oxygen ions in B is very similar to that observed for configuration A. However, unlike configuration A, the cerium ions not only relax upwards in the z-direction, but also relax in the xy plane due to the defect symmetry. In addition, there is a greater polarisation of the cation and anion surface planes; about 7% downwards

for the oxygen shells (relative to their relaxed cores) and 6% in the xy plane for the cerium shells. The result of this relaxation, combined with the original arrangement of the ions, is the formation of a flatter surface; such faces tend to be slower growing.

The formation of cerium defects (configuration C), either vacancies or interstitials, results in a less stable surface. The primary reason for this is that cerium defects result in large electric fields due to their +4 charge and small ionic radii. Also, associated with the high charge of the cerium ions is a high vacancy formation energy; a Ce vacancy in the bulk requires approximately 80eV to form compared to 16 eV for an oxygen vacancy. Thus one would not expect such cation terminated surfaces to be significant.

The (331) plane Figure 5.15 shows the relaxation of the (331) surface. This is a highly stepped face and is seen in the equilibrium morphology if the Butler potentials are used. The relaxation seen is quite complex and can be explained more easily if one studies the cerium atoms labelled (i) and (ii) and the oxygen atoms labelled a), b), c), d), and e). During relaxation cerium atom (i) rearranges to be further down into the surface. This effectively increases its coordination and decreases the electric field on the bulk. The (ii) set of cerium atoms remain almost at their original lattice positions. This can be understood in terms of the oxygen relaxations; the most distinct movement is the increase in the distance between atoms b and c. Such movement places these atoms further into the bulk and reduces the angle between atoms c and d. The change in angle between atoms c and d results in an increase in the coordination of the (ii) set of cerium atoms, which is why they do not relax further into the surface. Overall the relaxation also reduces the angularity of the face, resulting in a smoother electric field over the surface. Note, the relaxation of the ions

does not proceed to a great depth, and is only detectable in the first and second layers. The same dependence of relaxation with has recently been seen reported in TiO_2 [128, 129] using high quality quantum mechanical techniques.

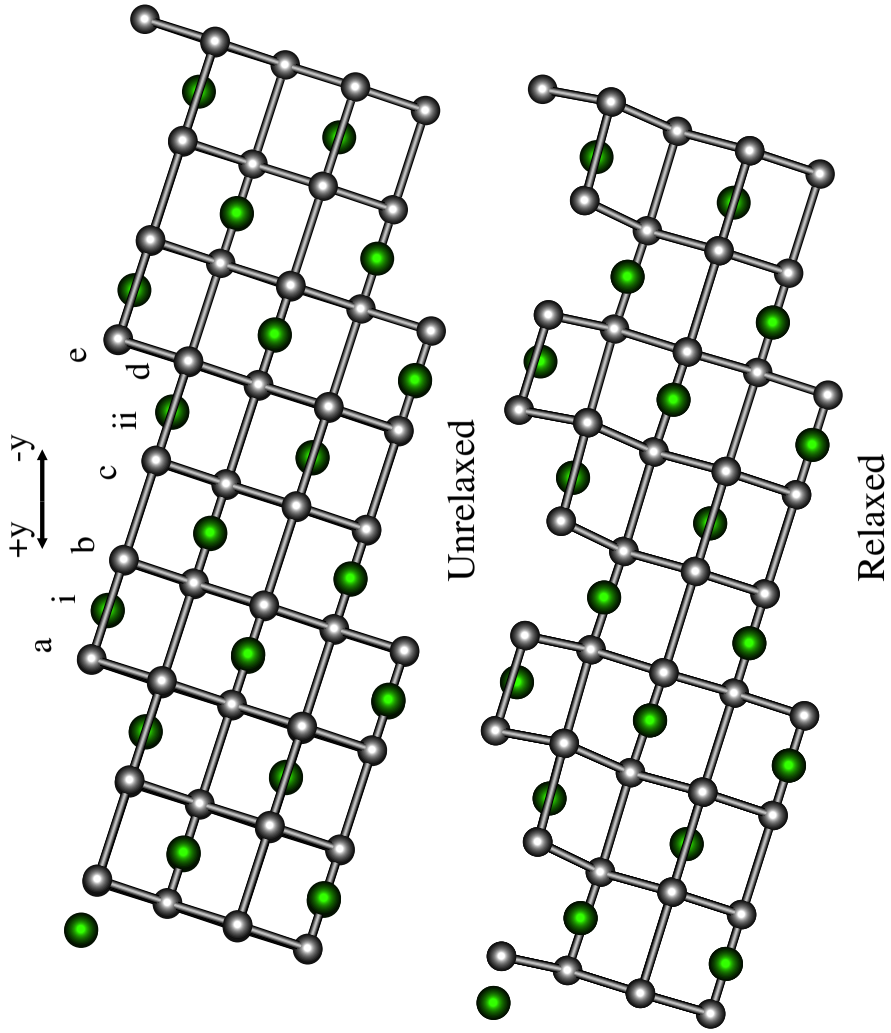

Figure 5.15: Surface structure of the 331 surface when viewed side on.

5.10 The Significance of Orientation on Dipole Neutralising Defects

It was mentioned in the discussion of the (200) surface structure that the orientation of the defect neutralising species affected the surface energy of the face. In the present section we investigate the effect of defect orientation on the other type III surfaces of CeO_2 using potential 1.

(210) The oxygen ion can be orientated in two unique ways. Table 5.6 and Figure 5.16 show the two possible orientations of the defect and their surface energies. The first configuration has defects approximately 6.05Å apart and the second has defects 6.63Å from each other. The second configuration has a lower unrelaxed and relaxed surface energy. This would be expected given that the ions are further apart, and hence they will repel each other to a lesser extent.

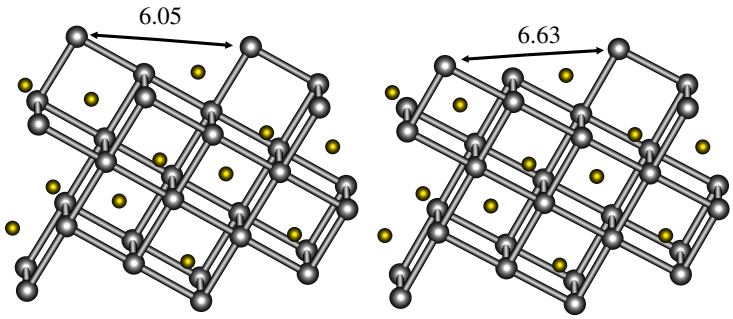

Figure 5.16: The defect orientations for the (210) surface. Distances in Ångstroms

(210) Surface	Surface Energy (Jm^{-2})	
Configuration	Unrelaxed	Relaxed
A	5.70	2.45
B	5.68	2.41

Table 5.6: Surface energies for the defect orientations on the (210) surface.

(221) This surface, like all the other type III faces studied, has two possible orientations for the two dipole neutralising defects; one where the ions are in line with each other, the other where they are diagonally orientated. The results (Figure 5.17 and Table 5.7), as inferred from the (210) and (200) faces show that configuration A, where the ions are diagonally orientated, has a significantly lower unrelaxed surface energy. Unexpectedly, this correlation does not carry through to the relaxed surface, where configuration B is slightly lower in energy.

(221) Surface	Surface Energy (Jm^{-2})	
Configuration	Unrelaxed	Relaxed
A	12.67	1.79
B	12.78	1.71

Table 5.7: Surface energies for the defect orientations on the (221) surface

(320) The two configurations are 9.75Å and 10.12Å apart (Figure 5.18). Unusually, both the surfaces have the same unrelaxed energies (Table 5.8). After relaxation, the 1st cluster is more energetically stable even though the ions are closer together. Clearly, the unrelaxed energies are equivalent as the distance between the defects is now large enough large that the inter-defect interaction energy is small.

(322) There are two possible orientations for the defects, Figure 5.19). From Table 5.9 one can see the configuration where the ions are further apart is not only less

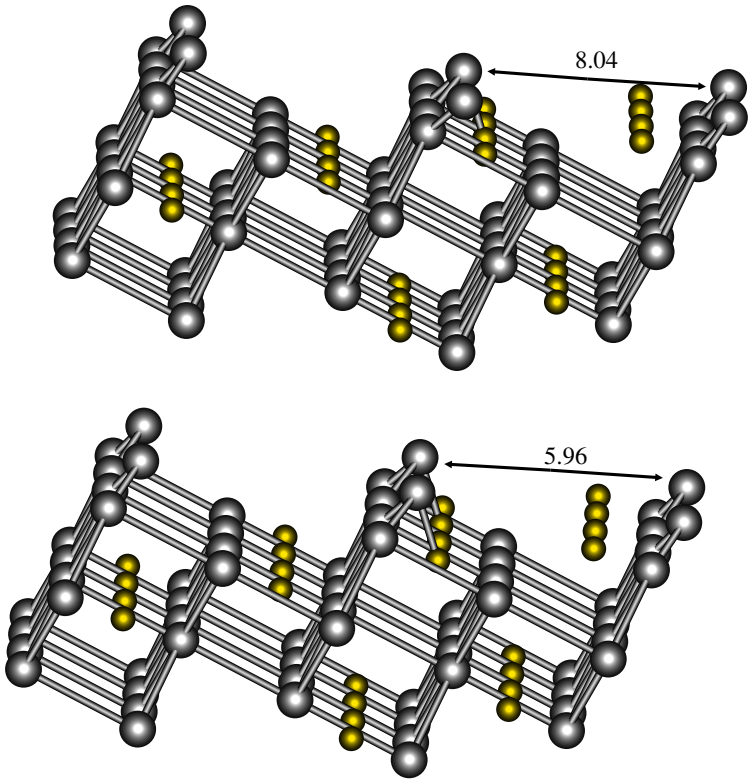

Figure 5.17: The defect orientations for the (221) surface. Distances in Ångstroms

(320) Surface	Surface Energy (Jm^{-2})	
Configuration	Unrelaxed	Relaxed
A	11.53	2.31
B	11.53	2.45

Table 5.8: Surface energies for the defect orientations on the (320) surface

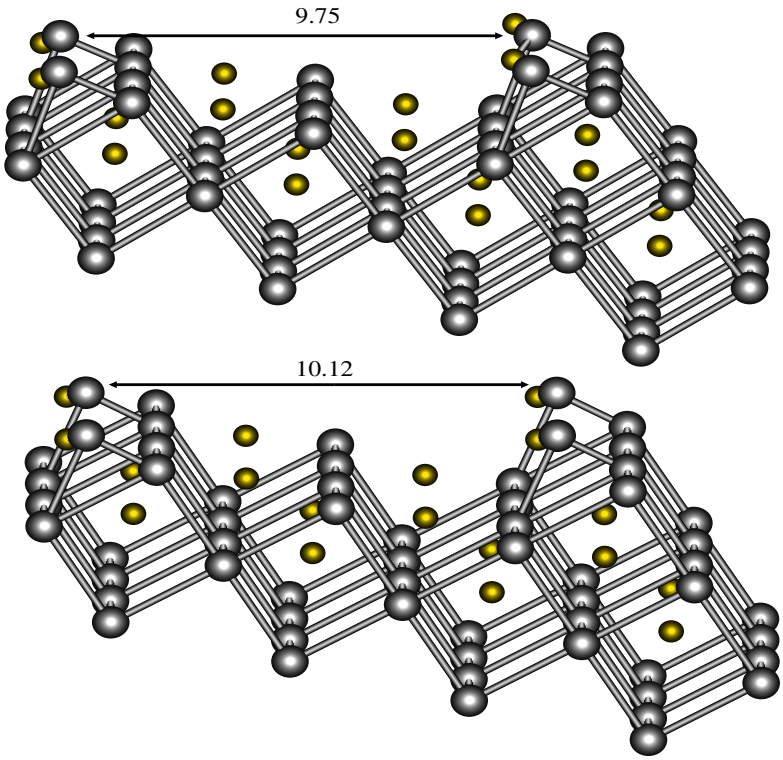

Figure 5.18: The defect orientations for the (320) surface. Distances in Ångstroms

favourable but actually destabilises the surface. Such a phenomenon can be explained by the fact that although the defects within the repeat unit are further apart, the defects of adjacent cells are much closer together.

(322) Surface	Surface Energy (Jm^{-2})	
Configuration	Unrelaxed	Relaxed
A	-38.19	Unstable
B	11.58	2.05

Table 5.9: Surface energies for the defect orientations on the (322) surface

(410) The possible orientations are shown in Figure 5.20. It can be seen that as with the (320) face, both configurations have similar energies before relaxation (Table 5.10). After relaxation, the configuration where the defects are in line (and hence closer to each other) is more stable. Again the reason for the unrelaxed energies being equivalent is that the defects are too far apart to interact significantly.

Overall, it can be concluded that the orientation of the dipole neutralising defects will only affect the surface energies of low index faces such as the (200) and (210). In these cases, the ions are close enough to interact with each other. For higher index faces the effect is negligible. After relaxation, the assumption that the configuration where the ions are furthest apart will be the most stable becomes less valid as certain high index faces undergo large surface rearrangements.

(410) Surface	Surface Energy (Jm^{-2})	
Configuration	Unrelaxed	Relaxed
A	13.61	3.82
B	13.62	2.77

Table 5.10: Surface energies for the defect orientations on the (410) surface

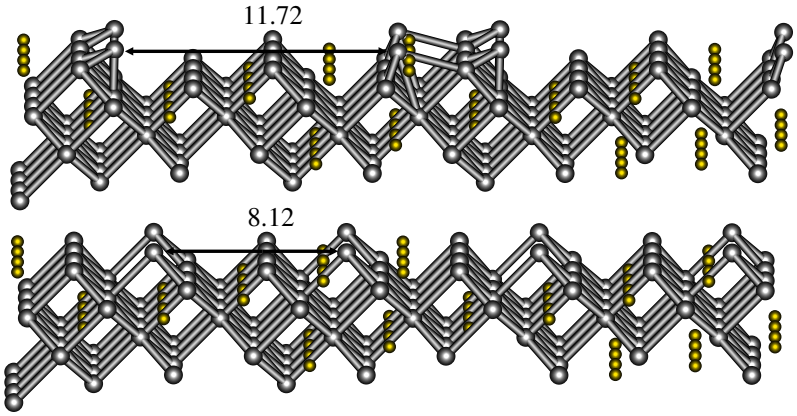

Figure 5.19: The defect orientations for the (322) surface. Distances in Ångstroms.

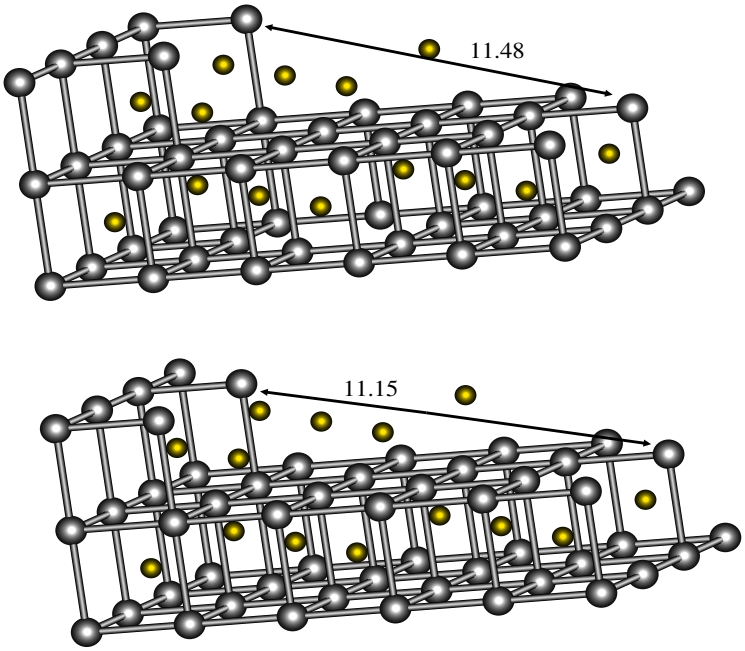

Figure 5.20: The defect orientations for the (410) surface. Distances in Ångstroms.

5.11 Surface Relaxation; the potential dependence

Here we study the dependence of the surface relaxation and ion polarisation on the choice of interatomic potential. We examine the morphologically important (111) face and the high index (331) surface with particular attention to ion relaxation as a function of depth from the surface. In all cases we discuss the displacement of ion shells from their perfect lattice positions, the core displacement on the other hand is relative to the relaxed associated shell. This approach is physically justified since the cores are connected to their respective shells by a harmonic spring and only interact electrostatically with other species. The shells on the other hand are coupled to other ions through the short range interactions.

(111) - Figures 5.21 and 5.22 show the displacement of the O^{2-} ions (i.e. the cores and shells). A positive value implies a displacement outwards to the free surface, a negative value a relaxation into the bulk. For both cores and shells below 6Å the magnitude of the displacements are small (i.e. less than 0.01Å). Above 6Å, although the displacements are still not large (compared with the (331) surface) there is a distinct difference between the predictions of the three potentials. The shell relaxation for the Butler model is the smallest and those for potential 1 and 2 are very similar. However, the relaxed shell displacements of the O^{2-} shell, for the Butler potential set, is balanced by the larger O^{2-} core displacement.

In the case of Ce^{4+} cores and shells (Figures 5.23 and 5.24), again the displacements are small for ions below 4Å, i.e. for all but the outer most ions. In the case of the shells, all of the outer ions, for all three potential sets, polarise into the surface. The similarity is due to the total charge of the ions (i.e 4+) being coupled to all other

ions via the shell. However, the cores show quite a different behaviour. For potential sets 1 and 2, the positive cores move into the surface but for the Butler model the negatively charged core polarises out of the surface. Nevertheless, the magnitude of the polarisation is very similar. This is understood if the physical nature of the core/shell model is examined. The electric field gradient at the Ce^{4+} site on a (111) surface will act to displace a positive charge into the surface. Therefore, the negative Butler core is displaced out but the positive shell is displaced inwards. The result is that the core stays practically unmoved from the perfect lattice site. Conversely, the positive cores of potential models 1 and 2 are displaced inwards and since the shell charge, though negative, is small it is drawn into the bulk through the coupling to the core. This overall displacement of the shells inwards is compounded by the inward relaxation of the outer oxygen ions, which interact via the shells. This emphasises the importance of considering the shell displacements as physically significant quantities. It therefore also questions the usefulness of a positive shell / negative core model in this regard.

Despite the differences in magnitude between the three potential models, the direction of the ion displacements as defined by the shells is the same; an alternating negative and positive pattern of displacement for Ce^{4+} layers and negative, negative, positive, positive for the O^{2-} layers.

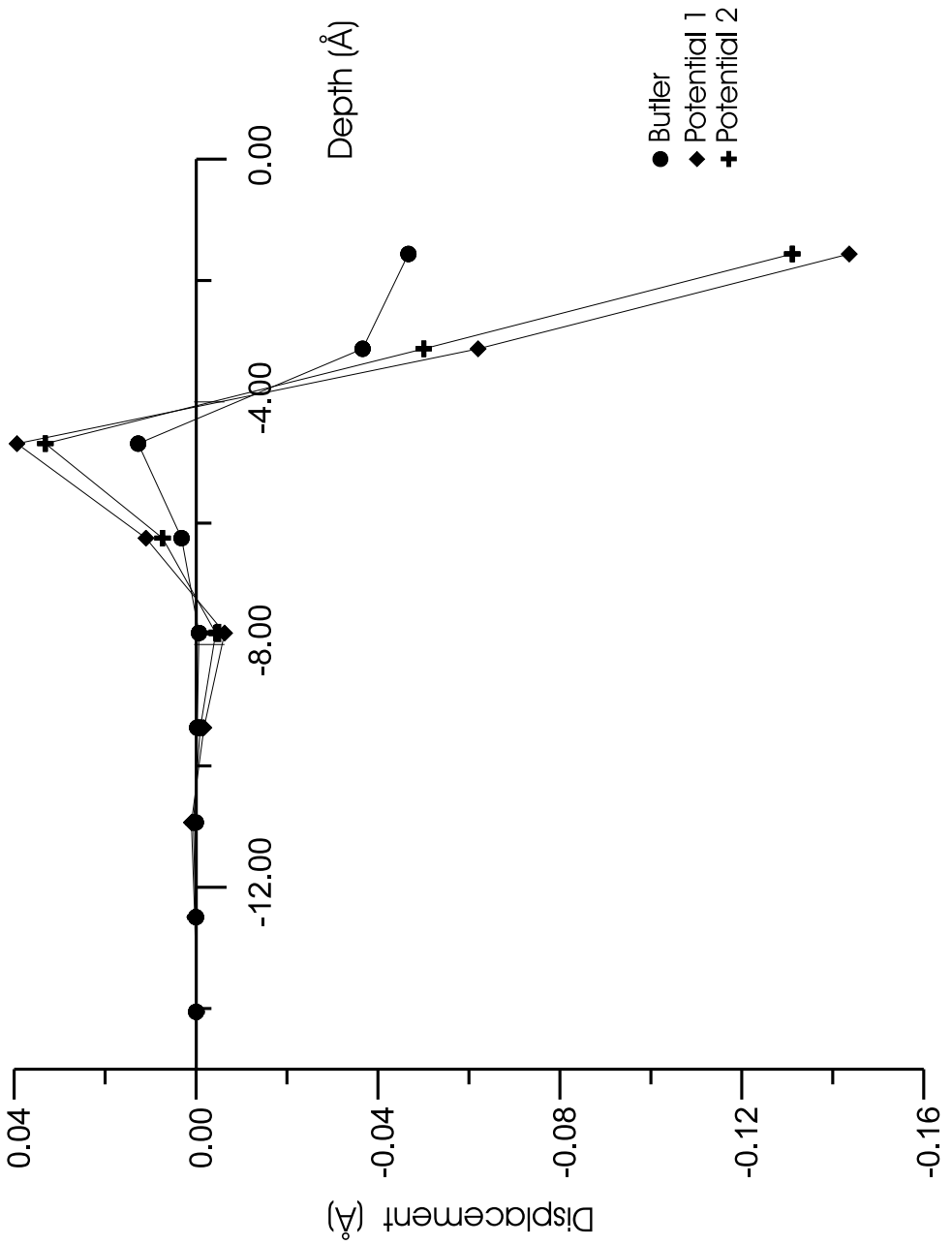

Figure 5.21: Displacement of oxygen shells with respect to their original positions on the (111) surface

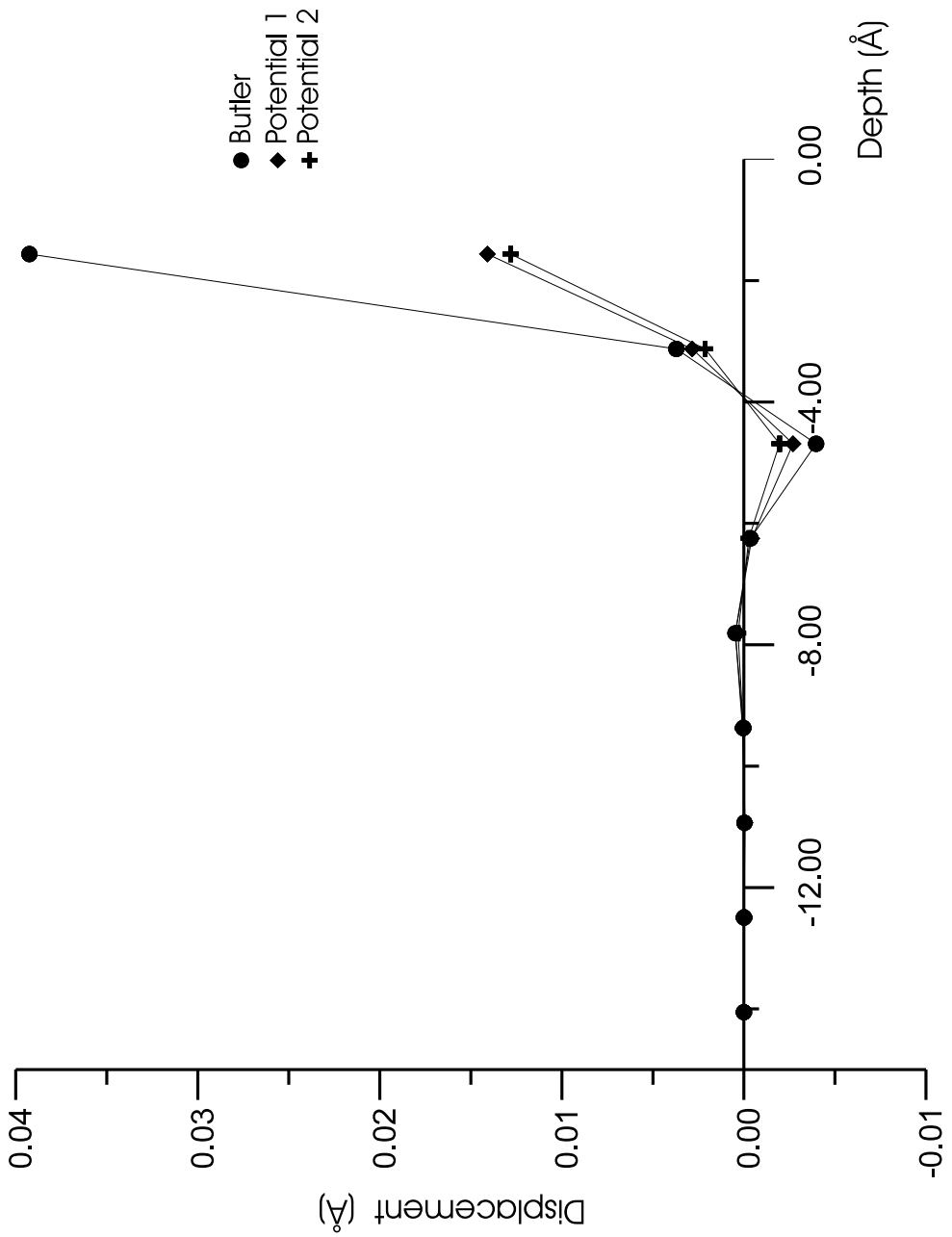

Figure 5.22: Displacement of oxygen cores relative to their relaxed shell positions on the (111) surface

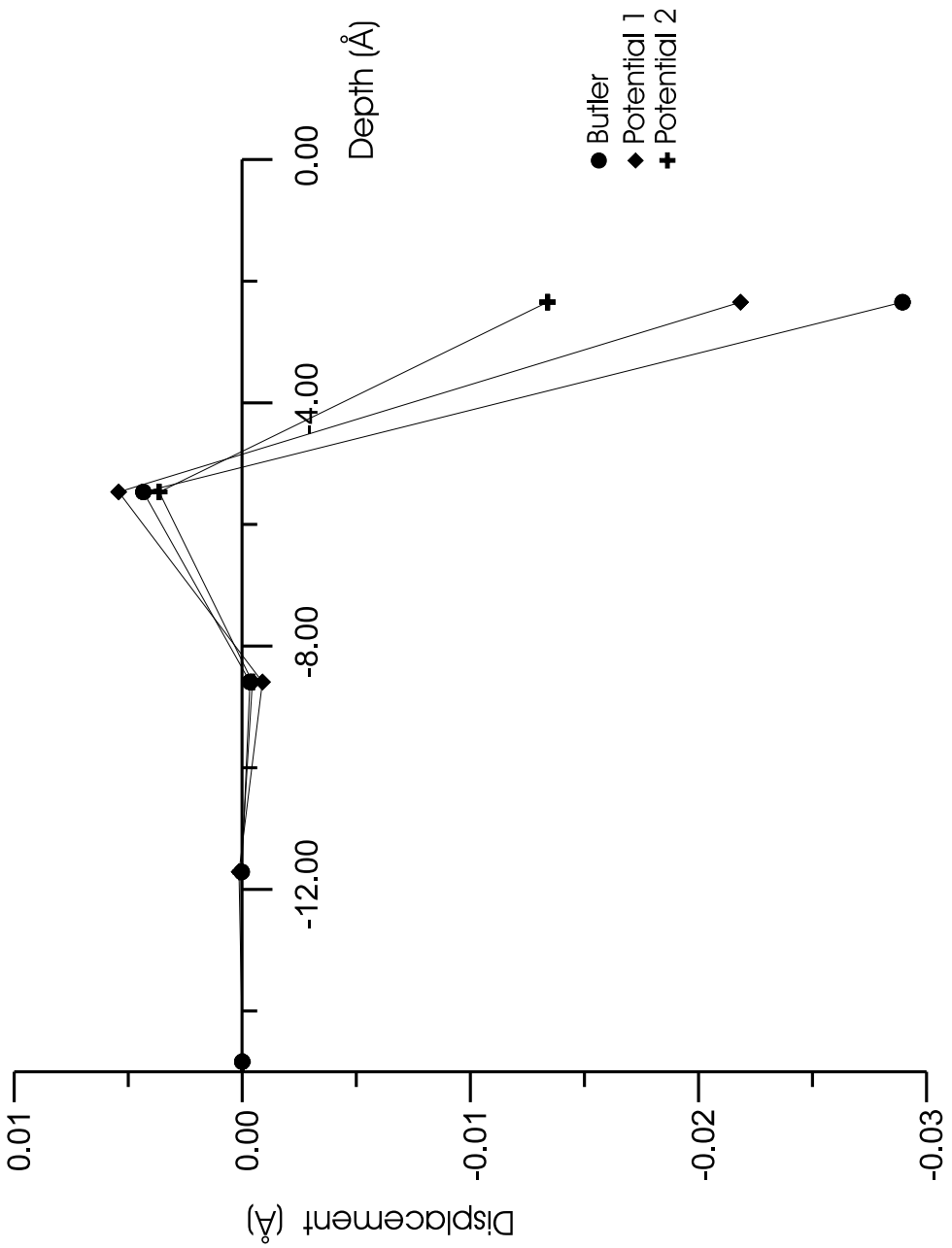

Figure 5.23: Displacement of cerium shells with respect to their original positions on the (111) surface

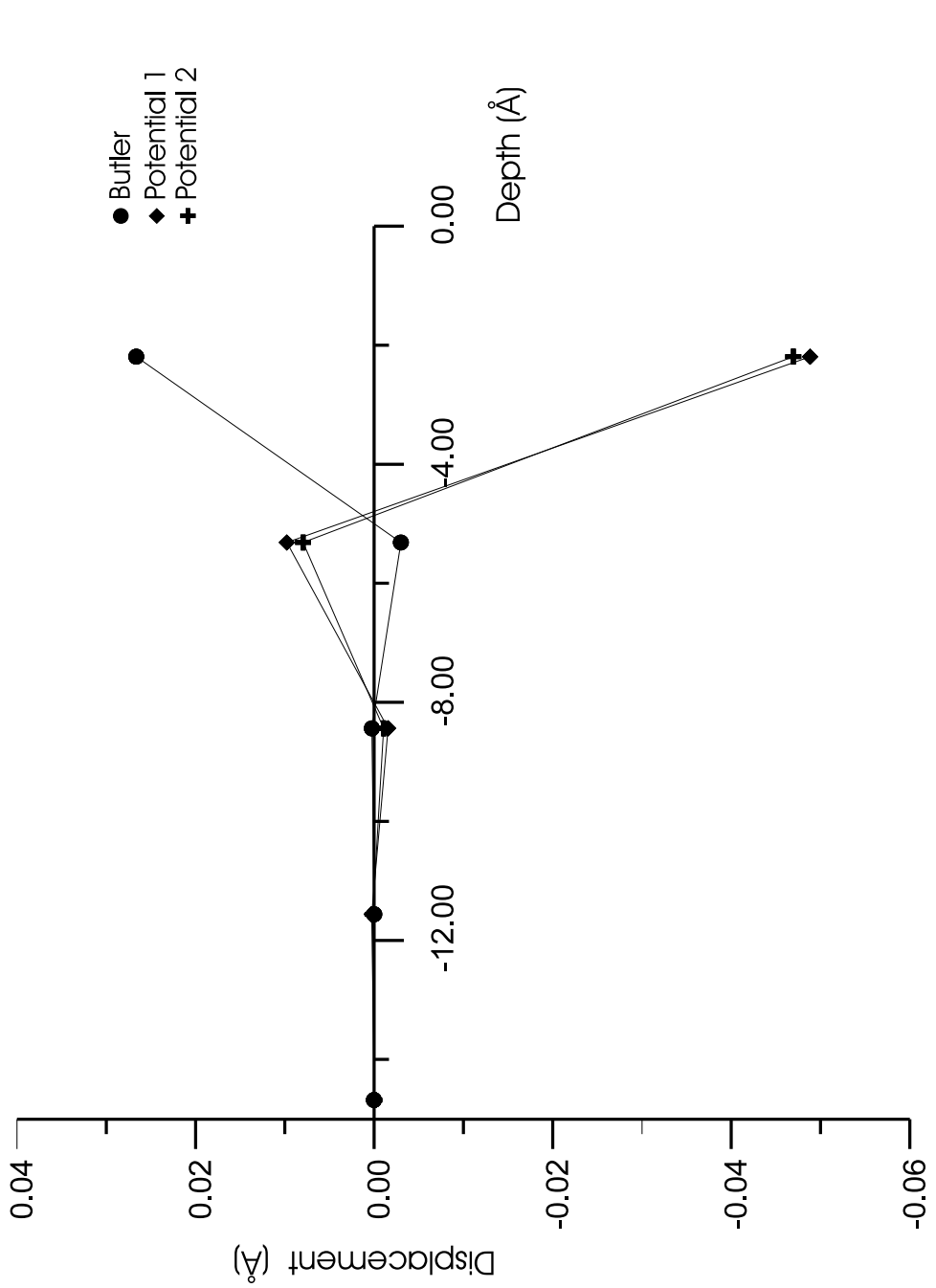

Figure 5.24: Displacement of cerium cores relative to their relaxed shell positions on the (111) surface

(331) - This high index face shows a more complex behaviour: in addition to the relaxation in the z-direction there is also movement in the y-direction which runs parallel to the surface steps. Hence, some of the ions, particularly those at low coordinate sites, such as on the corners of steps, will be subjected to unsymmetric forces. No relaxation is seen in the x-direction as a result of the symmetric surface structure in this direction.

Figure 5.25 shows the displacement of the cerium ions in the z-direction (the shells with respect to their perfect lattice positions). A negative movement indicates a displacement into the bulk, while a positive displacement implies a movement toward the surface. From the graph it is immediately clear why the Butler potential is not adequate to model high index faces. While the new potentials show a negligible relaxation below 5Å, the ions in the Butler model are still relaxing, and show a significant movement well into the bulk (approximately 12Å). However, the overall relaxation trends seen are very similar for all three sets of potentials, with all of them showing an oscillatory relaxation as a function of depth, with the Butler model being a particularly extreme case.

The polarisation of the cerium ions (Figure 5.26) show that below 3Å the polarisation is negligible. Above this depth, the polarisation is analogous to that seen for the (111) surface. In the first layer, the cores of the Butler model polarise up towards the surface and are about 0.04Å away from their perfect lattice positions. Potential 1 and potential 2 polarise downwards into the bulk, however, their shells on the other hand relax toward the surface. Hence, the cores are about 0.2Å away from their original positions. This is analogous to the behaviour seen for the (111) surface with the negative species remaining closer to the original lattice position than the positive

species.

For the O^{2-} species (Figure 5.27), potential 1 and potential 2 show a negligible relaxation below 4.5Å. On the other hand, the behaviour in the surface layers above is quite complicated. The first three layers show a large movement into the bulk, between 0.10Å and 0.17Å. The subsequent layers show a positive relaxation towards the surface of about 0.05Å. The polarisation (Figure 5.28) of these two potentials models is small in the first three layers, and practically negligible in subsequent layers and is analogous to the shell relaxation .

The movement of the O^{2-} ions in the z-direction for the Butler model is completely different. The shell relaxation is a decaying oscillation with a considerable displacement, ≈ 0.17Å in the first 3/4 layers, which is clearly an unphysically large amount. Although, it is not shown on the graph for the sake of clarity, the relaxation tapers off at a depth of approximately 14.3Å. The core polarisation shows similar behaviour; however, the oscillation period is larger and the decay to zero much quicker. The polarisation is quite extreme, with the shells in the first layer barely remaining bound to the core. These observations add further weight to the argument that the Butler potentials are not appropriate for the simulation of high index planes where the electric field gradients are very large.

As mentioned previously the (331) face, in addition to showing movement in the z-direction, also shows a lateral movement in the y-direction. The relaxation and polarisations seen are similar to those in the z-direction. Figure 5.29 shows the relaxation of the cerium shells in the y-direction (parallel to the steps). A negative displacement indicates movements towards the bottom of a step and a positive displacement towards the top of a step (see axis in Figure 5.15). The trends seen in

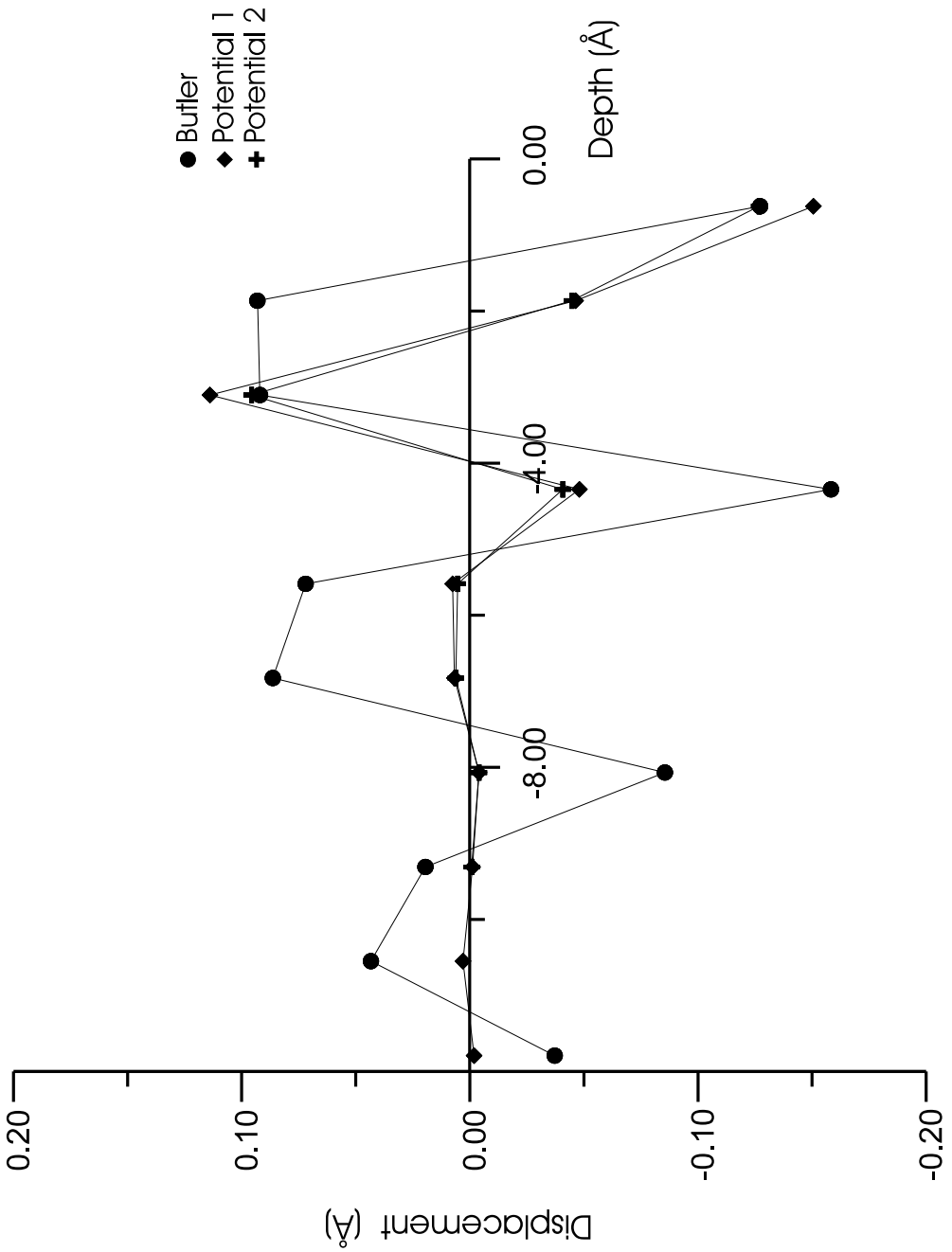

Figure 5.25: Displacement of cerium shells relative to their original positions in the z-direction

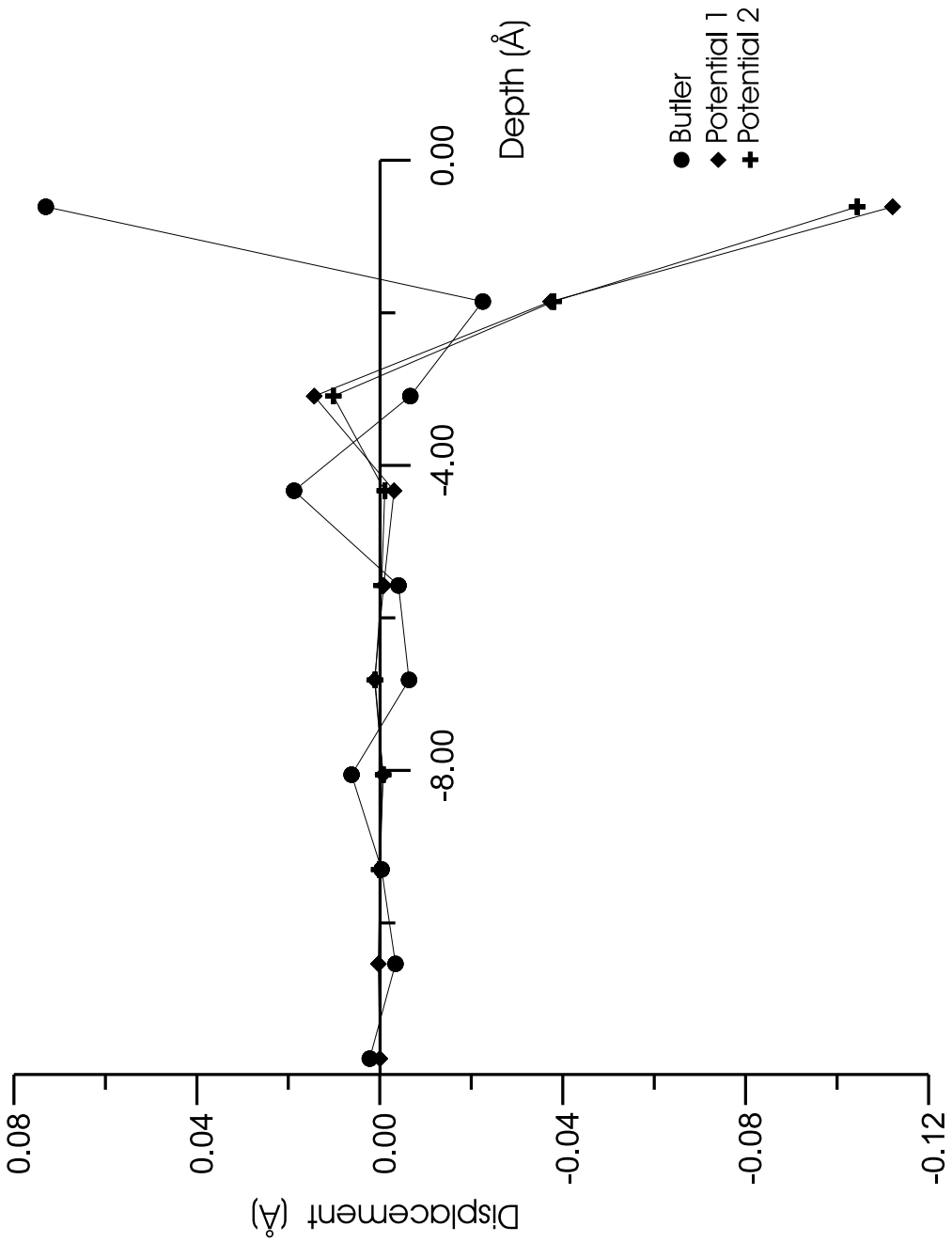

Figure 5.26: Displacement of cerium cores relative to their relaxed shells in the z-direction

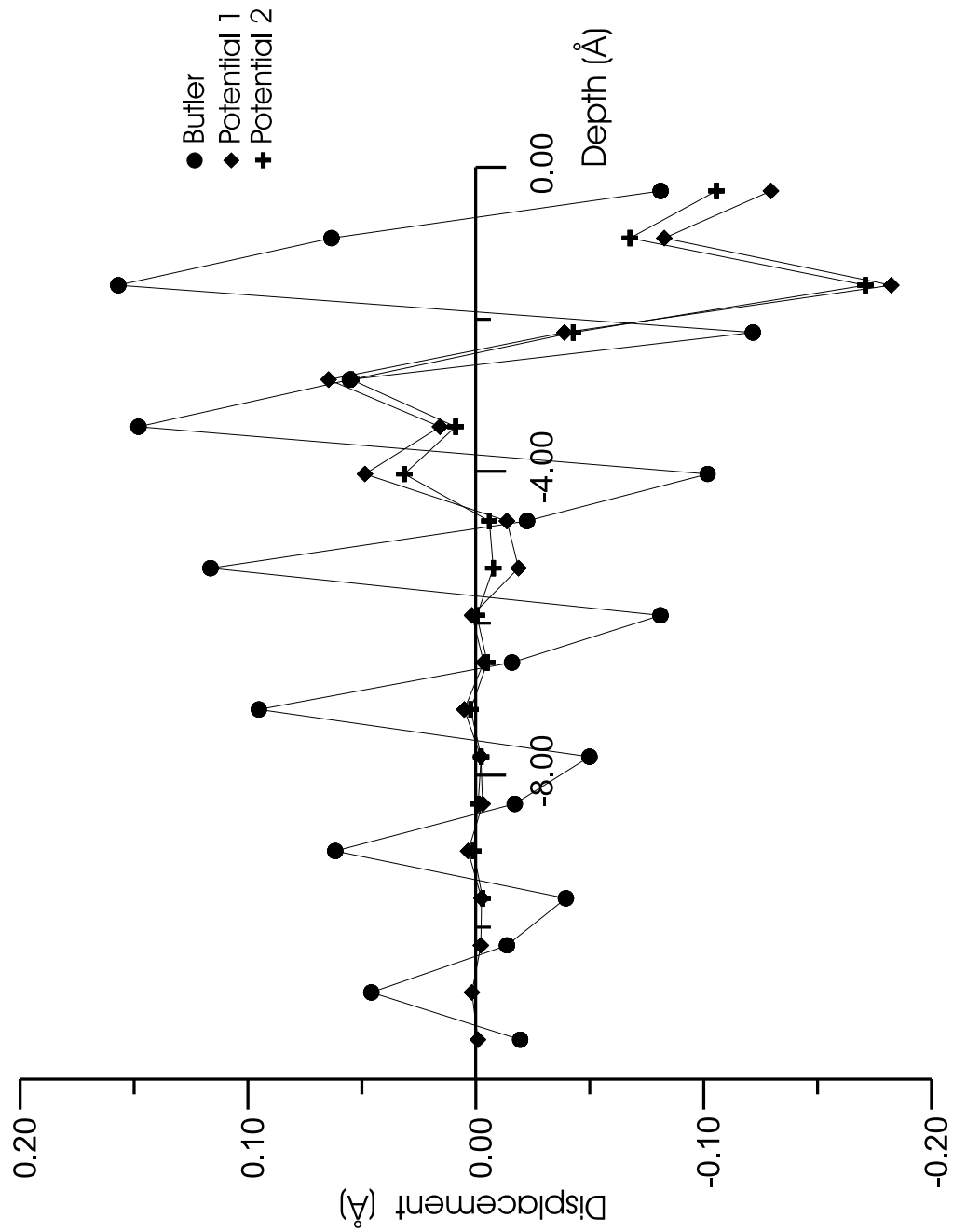

Figure 5.27: Displacement of oxygen shells relative to their original positions in the z-direction for the (331) surface

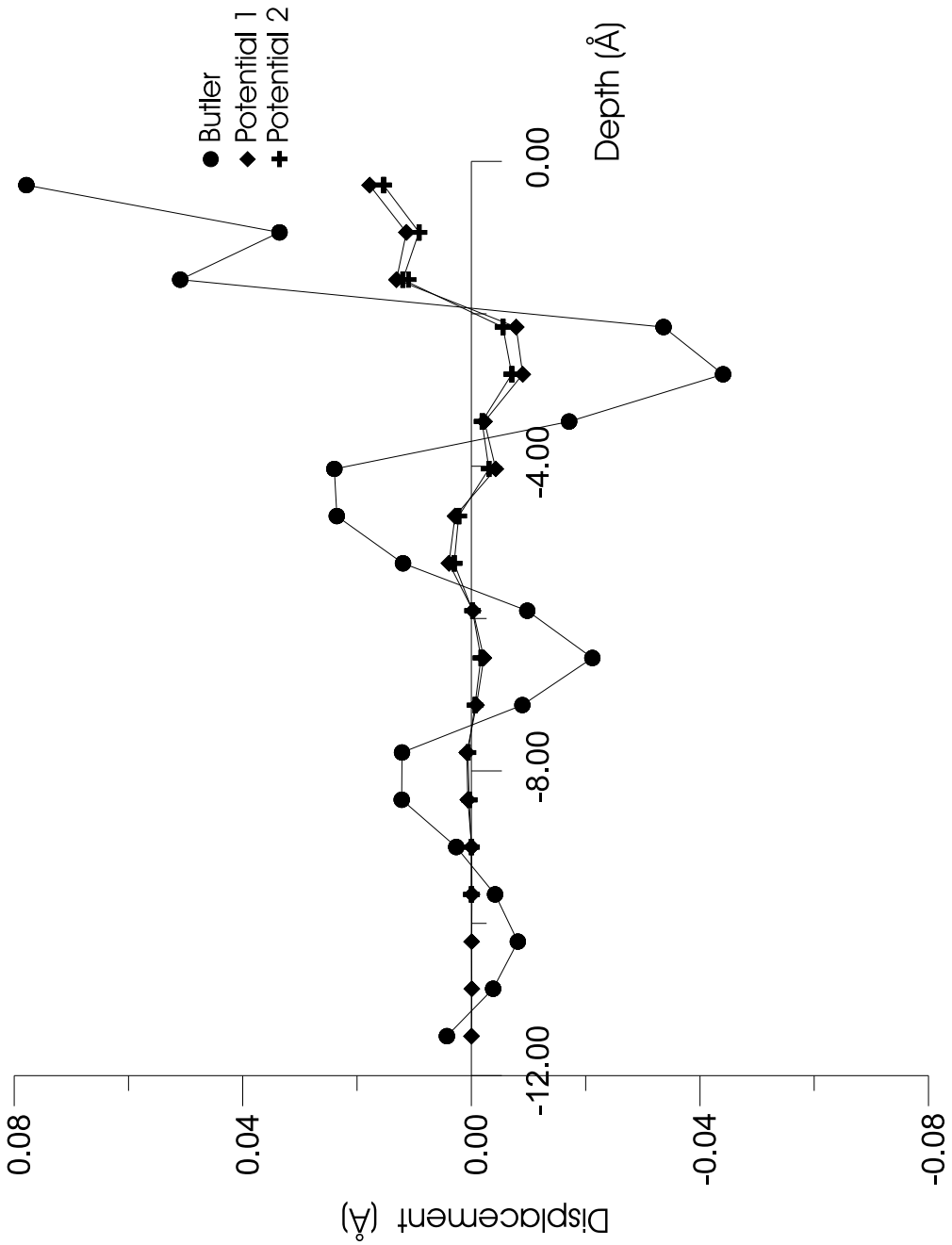

Figure 5.28: Displacement of oxygen cores relative to their relaxed shells in the z-direction for the (331) surface

the y-direction are very similar to that seen in the z-direction for the Ce cores. The newer potential 1 and potential 2 on the whole relax to a lesser extent than the Butler potential and taper off more rapidly. The Butler potentials continue to oscillate to a depth of about 12Å. The polarisation (the displacement of the cores with respect to their relaxed shells) in the y-direction reinforces (Figure 5.30) the observations made about polarisation in the z-direction; the positive species moves to a lesser extent than the negative species.

The oxygen ions relax significantly (Figure 5.31) more than the cerium ions, with the largest being 0.45Å (an even larger relaxation than in the z-direction). Clearly, such behaviour is a result of the surface structure; the surface steps run parallel to the y-direction and are defined by the oxygen sub-lattice. Thus, the oxygen atoms will relax to a greater degree in this direction as they attempt to increase their coordination. This effect is not as pronounced for the Ce^{4+} atoms as they generally have a higher and more symmetric coordination. The three potentials behave in a very similar manner below 3.00Å. However, above this depth they are significantly different. In the 3rd and 4th layers, ions modelled with the potentials 1 and 2 are moving in a different direction to the Butler potential. Both potentials 1 and potentials 2 relax out toward the top of the step, while the Butler potential moves inwards, albeit by a significantly smaller amount. In the first and second layers, the three potentials relax in the same direction. However, potentials 1 and 2 relax to a lesser extent.

The polarisation (Figure 5.32) in the y-direction replicates that seen in z-direction. Both potential 1 and 2 show no significant polarisation, and below 5.00Å it is negligible. On the other hand the Butler model shows a very significant polarisation, especially in the first 3 to 4 layers. The overall trend in the polarisation is again a

decaying oscillation, whose direction is similar to that seen in potentials 1 and 2.

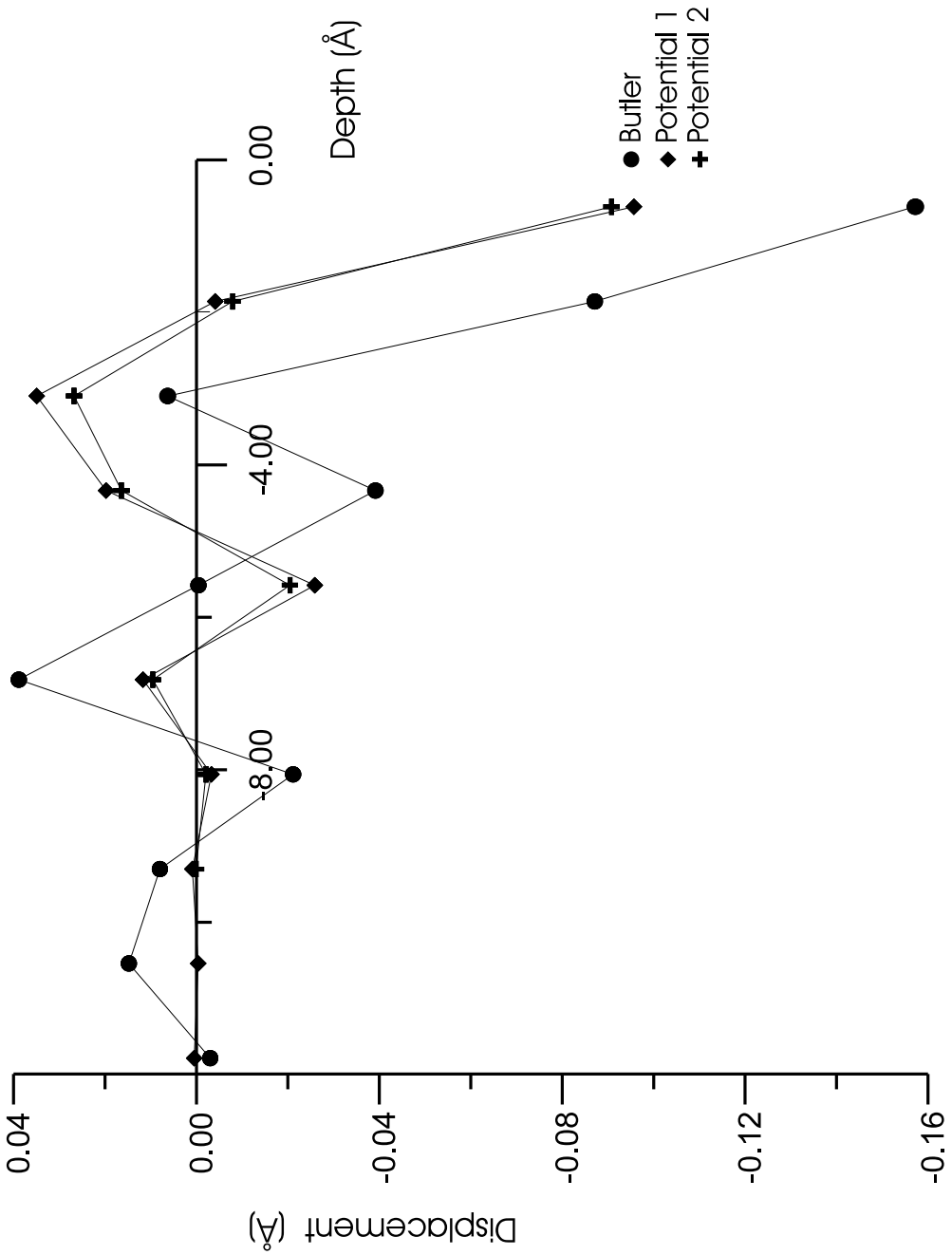

Figure 5.29: Displacement of cerium shells relative to their original positions in the y-direction

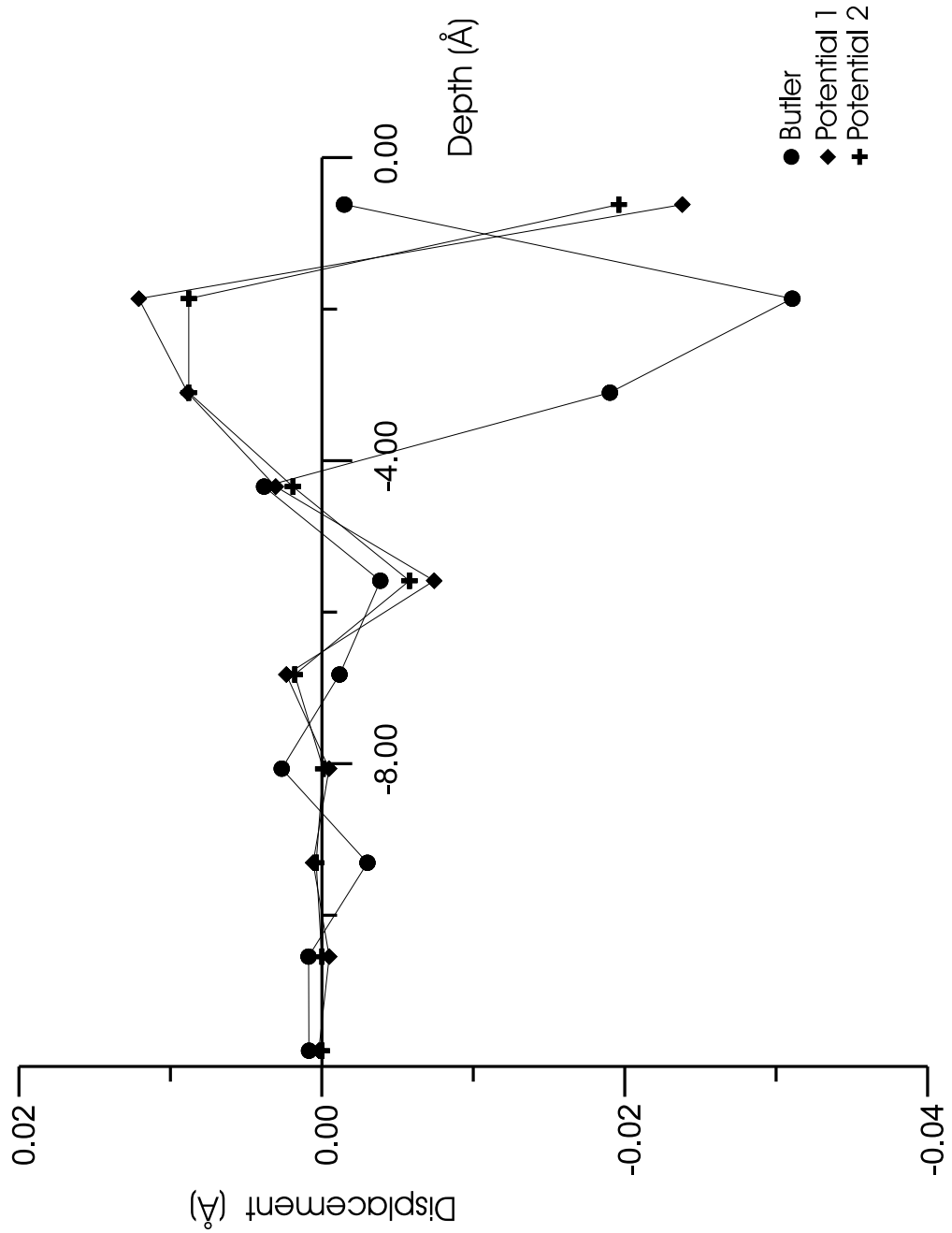

Figure 5.30: Displacement of cerium cores relative to their relaxed shells in the y-direction

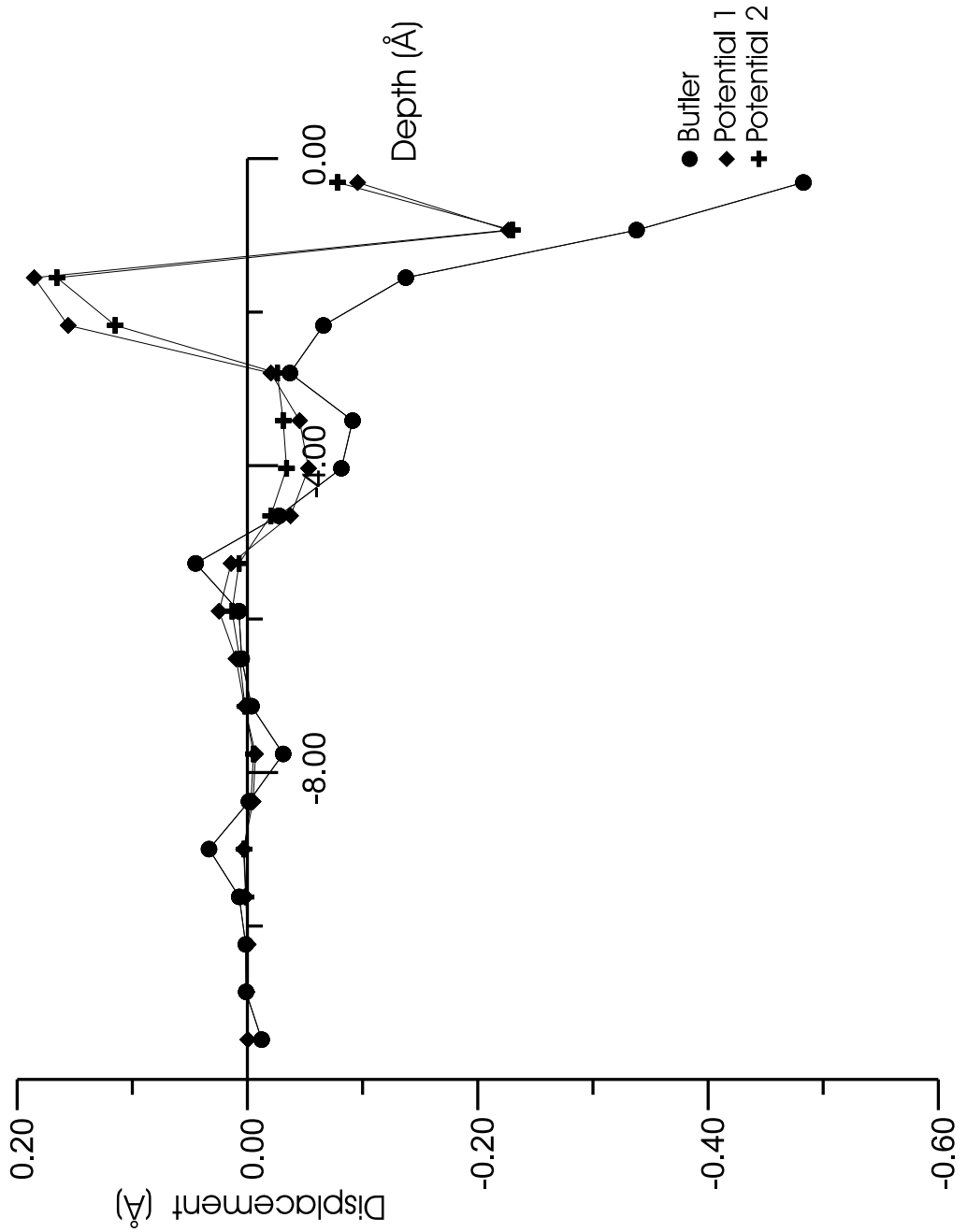

Figure 5.31: Displacement of oxygen shells relative to their original positions in the y-direction

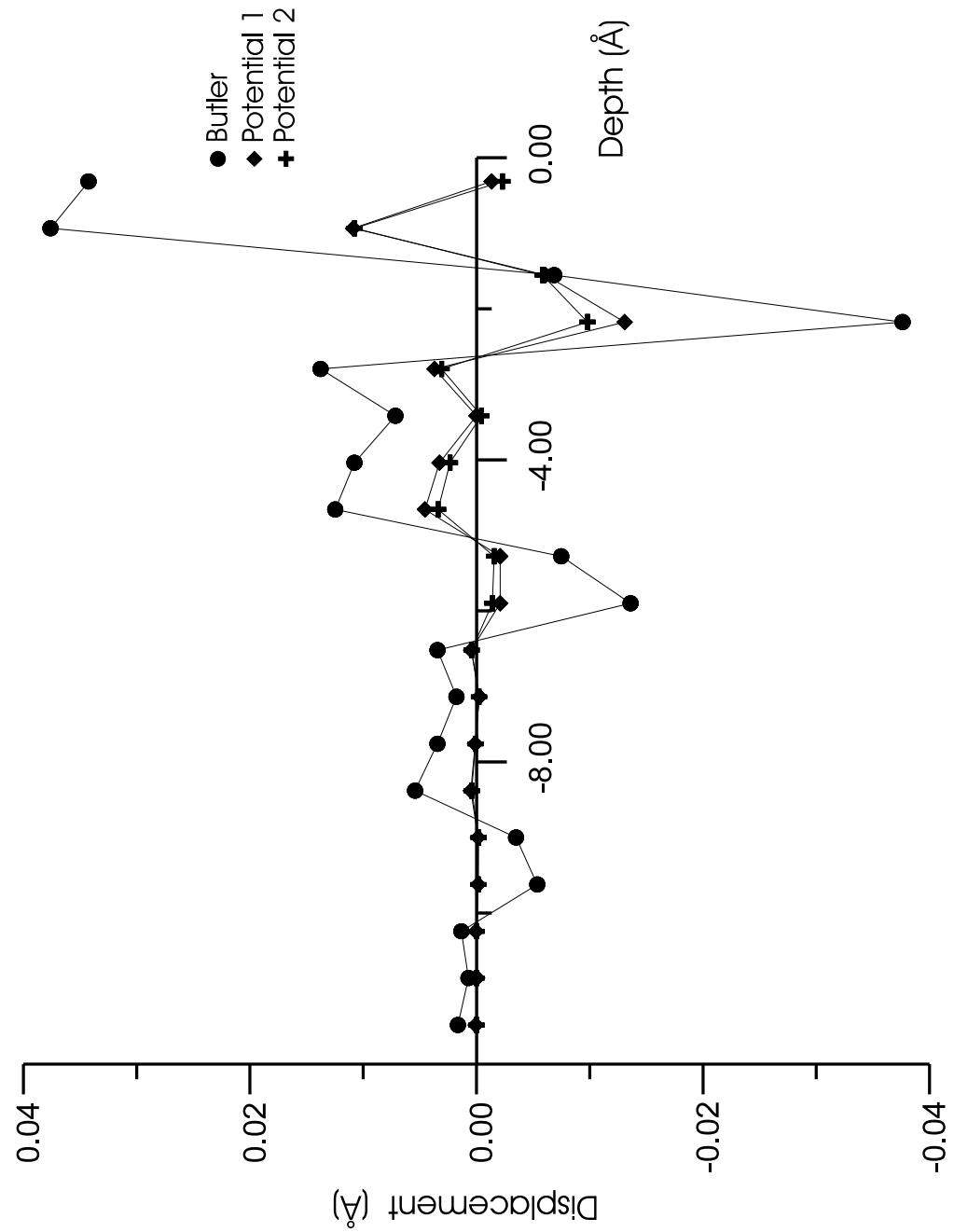

Figure 5.32: Displacement of oxygen cores relative to their relaxed shells in the y-direction

5.12 Bond Density

It was shown from Figure 5.9 that the surface energy as a function of misorientation angle was relatively independent of the choice of short range potential. Thus the curve seen must arise for a physical reason. A likely origin for the observed surface energy relationship is the number of bonds that are broken when the surface is created by cleaving the crystal. Figure 5.33 shows the number of O^{2-} - O^{2-} and Ce^{4+} - O^{2-} bonds that are broken per unit area when the unrelaxed surface is created for the (01a) series of planes. It is clear from the diagram that in both cases the minimum lies at 45°, which is analogous to that seen for the surface energy. Further weight is added to this postulation in that it may be able to explain the reason the (310) surface has a higher energy than the (210) and (410) surfaces. When the density of O^{2-} - O^{2-} bonds broken is examined it seen that more of these bonds are broken on the (310) surface than either the (410) or (210) surface.

At present, time constraints have not permitted an analysis of the (11a) family of planes. However, should they reproduce the pattern seen in Figure 5.8 further weight would be added to this correlation.

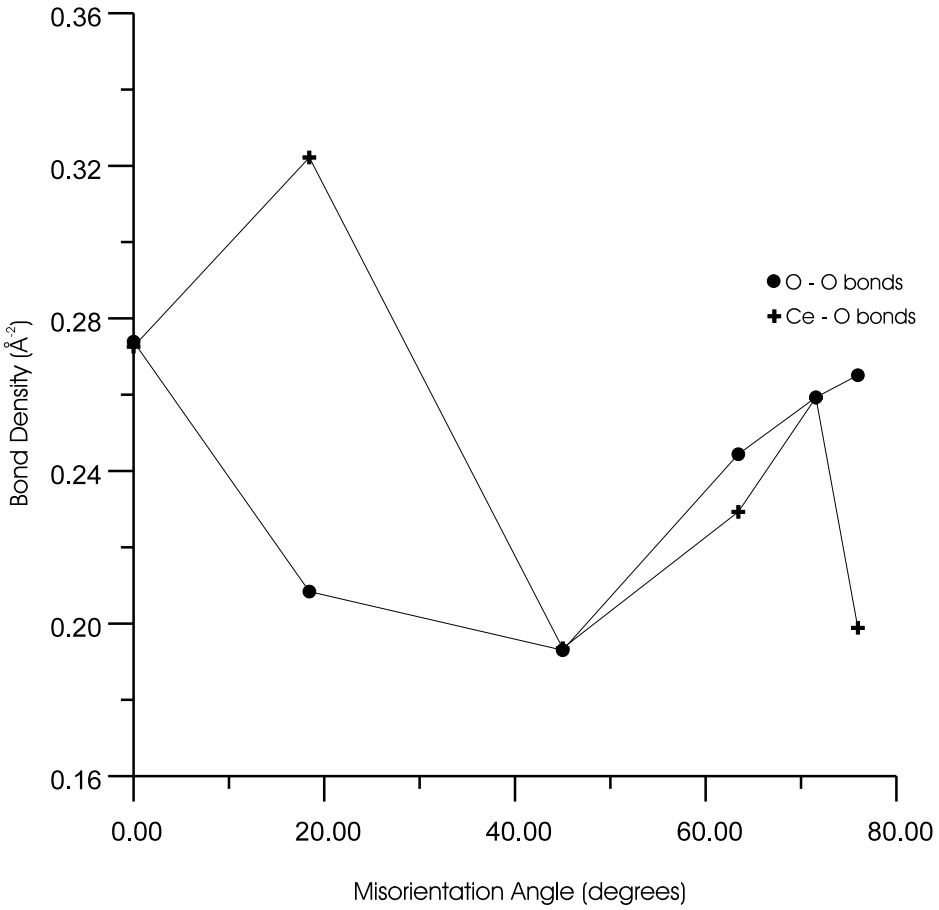

Figure 5.33: Bond Density as a function of misorientation angle

5.13 Summary

For a given surface, the three interatomic potential sets used in this study give rise to significant differences in surface energies. Despite this, the way that energy changes as a function of surface orientation is maintained for all three potentials. As such, predictions of crystal morphology are, largely potential independent. The exception to this is the Butler equilibrium morphology which shows (331) and (210) facets. The presence of these facets is explained by the analysis of the relaxation and polarisations of the ions a function of depth for the three potentials. This shows that the Butler model is inadequate for high index surfaces. As such, the present work has highlighted some weakness in the derivation of interatomic potentials for surface studies that are based only on the bulk crystal data from one compound. Nevertheless, two of the models (potential 1 and 2) are able to reproduce surface structure without recourse to higher order polarisability force constants. This is in part due to the way that the oxygen - oxygen potential was derived for a series of materials and hence over a wider range of interatomic separations. The penalty for this is that the perfect lattice properties for a specific material are not reproduced as well. Additionally, the present chapter has examined the orientation of defects on a range of type III surfaces. The results indicate that the orientation of such defects is only significant for low index faces where the defects are close enough for short range effects to be important. Initial studies of the number of bonds broken per unit area when a surface is created from a bulk crystal indicate that there is a strong correlation with the surface energy.